1537

MODELS OF JUPITER'S ATMOSPHERE

BY

GARY CHARLES GOODMAN
B.S., California Institute of Technology, 1960
M.S., University of Illinois, 1964

THESIS

Submitted in partial fulfillment of the requirements
for the degree of Doctor of Philosophy in Astronomy
in the Graduate College of the
University of Illinois, 1969

Urbana, Illinois

UNIVERSITY OF ILLINOIS

THE GRADUATE COLLEGE

June 1969

I HEREBY RECOMMEND THAT THE THESIS PREPARED UNDER MY SUPERVISION BY GARY CHARLES GOODMAN

ENTITLED MODELS OF JUPITER'S ATMOSPHERE

BE ACCEPTED IN PARTIAL FULFILLMENT OF THE REQUIREMENTS FOR THE DEGREE OF DOCTOR OF PHILOSOPHY IN ASTRONOMY

G. C. Mortlie
In Charge of Thesis

G. C. Mortlie
Head of Department

Recommendation concurred in†

G. C. Mortlie
R. L. Schult
Julian H. Cole
S. P. Wyatt, Jr.
John R. Dickel

Committee on Final Examination†

† Required for doctor's degree but not for master's.

D517

ACKNOWLEDGEMENTS

I would like to express my gratitude to my advisor, Dr. John R. Dickel of the Department of Astronomy, for his guidance, encouragement, and suggestions throughout the period of research for this thesis. Many thanks are also extended to Dr. Larry Trafton for supplying me with the computer output for his model atmospheres and for the absorption coefficient of hydrogen, and to Dr. Paul Lee with whom many of the ideas presented in this thesis were discussed and thought out.

Figures 4.3 - 4.7 were done with the assistance of Paul Weston of the Coordinated Science Laboratory and his programs for graphical display.

I am also thankful to Mrs. Julie Anson for her help in the preparation of this thesis.

Finally I am deeply indebted to my many friends for the help and encouragement that they have given me throughout this thesis.

This work has been supported, in part, by the National Science Foundation, Contract Number GP-8161.

TABLE OF CONTENTS

Page

LIST OF FIGURES

Figure Page

1. Introduction

1.1 General

There are numerous clues to the structure of the Jovian atmosphere: the spectral features and reflectivity of the atmosphere, the spectrum of its thermal emission, the observed cloud structure with its color, turbulence, and non-uniform rotation rate, and the planet's mass, radius, and polar flattening. The actual atmospheric structure must be inferred from these clues by means of a valid theory for the observed features applied to a reasonable model for the atmosphere. The information gained in this way can then be used to make a more sophisticated model. Some types of observations require much more detailed models than do others in order to lead to realistic conclusions. In some cases the observations are difficult to make and have large uncertainties. Finally the theory itself may be inadequate to lead to unqualified conclusions. Thus, in spite of all these clues, there is still a great deal of uncertainty in our knowledge of such things as the composition of the atmosphere, the effective temperature (equivalent black body temperature), and the depth and nature of the clouds.

The purpose of this research has been to further improve Jovian model atmospheres and to compare the prediction from these models with the various types of observations which are available.

In particular these new models have been used to predict the thermal component of the microwave brightness temperature.

Some of the most pertinent observations and atmospheric models are discussed in the following sections.

1.2 Chemical Composition

a) General

The only molecules which have been positively identified spectroscopically in the Jovian atmosphere are hydrogen, methane, and ammonia. Owen (1965a,b) has examined the spectrum of Jupiter in the wavelength regions 7750 to 8800Å and has found no lines which could not be attributed to these molecules. Danielson (1966) observed Jupiter at low resolution in the 0.8 to 3.4μ region. He attributed all of the rather broad spectral features which were observed to these same molecules. Low resolution scans of Jupiter in the ultraviolet between 2000 and 3000Å were obtained by Stecher (1965). Greenspan and Owen (1967) ascribe the atmospheric reflectance in this spectral region to a Rayleigh scattering continuum due to H_2 with some absorption due to probably either NH_3 or H_2S. Absorption features observed at 2600Å and below 2100Å have not yet been definitely accounted for. Sagan (1968) believes that these absorptions may be due to small amounts of purines or pyramidines in the condensed phase. Other gases, which on the basis of cosmic abundances, are expected to exist in significant quantities in the Jovian atmosphere are He, Ne, and H_2O (Greenspan and Owen). Helium

and neon have no transitions in the observable portion of the Jovian spectrum, and water will be frozen out of the atmosphere untill well below the visible cloud layer. Still other gases, which might exist in small quantities, have been searched for without success (Spinrad and Trafton (1963), Owen (1965a), and Moroz (1966)).

The spectroscopic determination of the actual and relative atmospheric abundances of the different molecular species is difficult to obtain. The various values determined are summarized in Table 1.1 and discussed below. The problem is complicated by the cloud structure, about which more will be said in Section 1.4c. For lack of any definite knowledge of the shape and depth of the clouds and the distribution in size, density, and albedo of the scattering particles within them, a simplified model for the atmosphere and clouds has usually been used in the reduction of spectroscopic observations. This model consists of a clear (i.e. non-scattering) isothermal atmosphere overlying a discrete reflecting cloud level. Some authors have attempted to correct for scattering, as would occur from a thin diffuse cloud layer, by modifying the value of the effective air mass, or average slant path through the atmosphere. (Without scattering, the effective air mass is 4 if the spectroscope looks at the whole planet, but it is π if the spectroscope looks at only a strip through the center of the disk. Scattering can reduce this value to less than 2.)

Table 1.1

Summary of the Spectroscopic Determinations of the Abundances of the Major Constituents of the Jovian Atmosphere

Molecule	Abundance (km - amagats)	Wavelength (μ)	Reference
H_2	10.2	.2-.3	Stecher (1965)
	12	.2-.3	Greenspan and Owen (1967)
	110	.82	Tanaka (1966)
	68±14	.82, .64	Beckman (1967)
	85±15	.82, .64	Owen and Mason (1968)
	30±15	1.97	Moroz (1966)
	~45	2.4, 1.2	Danielson (1966)
CH_4	0.15	.6-.9	Kuiper (1952)
	0.1	.62	Beckman (1967)
	0.075	.9-1.7	Moroz (1966)
NH_3	0.003	1.26-1.58	Moroz (1966)
	~0.2	3	Danielson (1966)

b) Hydrogen

The hydrogen abundance has usually been determined from measurements of the equivalent widths of the highly saturated H_2 vibration-rotation quadrapole lines (Tanaka (1966), Beckmen (1967), and Owen and Mason (1968)). The lines which are generally used for the determinations are the 3-0 and 4-0 S(1) lines at 8150.7 and 6367.8Å respectively because they are free from blending with other lines. Other attempts to measure the H_2 abundance have been made from the collision-induced 1-0 and 2-0 bands of the H_2 spectrum centered at about 2.25 and 1.15 μ respectively (Danielson (1966), and Moroz (1966)). These determinations are very uncertain since the absorption coefficient has not been adequately studied in the laboratory, and the Jovian H_2-absorption features are strongly blended with absorption lines of NH_3 and CH_4.

Both Stecher (1965) and Greenspan and Owen (1967) have analyzed the ultraviolet reflectivity of Jupiter in terms of a model consisting of a Rayleigh scattering atmosphere of H_2 overlying a Lambert reflecting surface. They found a very low abundance of hydrogen which is most likely due to the fact that non-conservative scattering by particles limits the effective depth to which short wavelength radiation penetrates.

c) Methane

There is far less disparity in the measured values for the

abundance of methane than for hydrogen. Moroz (1966), observing in the infrared, found somewhat less CH_4 than did Kuiper (1952) and Beckman (1967) both observing in the red. Greenspan and Owen (1967) attribute this difference to scattering due to the cloud particles: "... absorption bands of moderate strength such as occur in the 1.0- to 2.5-μ region will correspond to much smaller amounts of gas than the very weak bands (such as used by Kuiper) ...".

d) Ammonia

The observed abundance for ammonia can give us little information on its relative abundance or mixing ratio in the lower atmosphere, i.e., beneath the cloud layer. This is because most of the ammonia has frozen out of the upper atmosphere. Specifically, the upper limit for the abundance of NH_3 at any level in the atmosphere is set by the NH_3 vapor pressure corresponding to the temperature of that level. Of course it may be lower than this. However, Greenspan and Owen showed that the amount of ammonia which they derive from Stecher's ultraviolet spectrum is in excellent agreement with the assumption that ammonia is 100% saturated above the clouds. Kuiper's value for the amount of NH_3 lying above the clouds, determined from lines in the red portion of the spectrum, is probably too high because scattering near the cloud layer, where the vapor pressure of ammonia is quite high, would greatly enhance the observed line strength. Danielson's measurement at 3μ appears to be too high even allowing for the fact that one might be

looking quite deep into the atmosphere at this wavelength. His value is almost two orders of magnitude higher than those obtained by Kuiper and by Moroz both of whom used observations of much higher resolution although in different spectral regions.

e) Cloud Top Pressure and the Abundance of Helium

Helium is believed to be the second most abundant constituent of the Jovian atmosphere, after hydrogen. However, the information that we have regarding its relative abundance is very indirect. Baum and Code (1953) observed the occultation of σ Arietis by Jupiter in 1952. From the rate of dimming of the starlight, they were able to measure the scale height of the Jovian atmosphere. The mean molecular weight of the atmosphere can be related to the scale height and the temperature of the occultation layer (stratosphere). A reasonable estimate can be made for the stratospheric temperature, but the observations themselves are very uncertain. The lower limit for the molecular weight is about 2.2. The upper limit from this observation is 4 to 5.

The measurement of "cloud top" pressure (Beckman (1967) and Owen and Mason (1968)) places a more restrictive constraint on the maximum value for the molecular weight. The cloud top pressure has been calculated from the measured widths of the weak pressure--broadened methane lines in the 6190-Å band. Again a simple reflecting model for the clouds has been used to relate the pressure at the cloud tops to the pressure in the laboratory which is required to give the observed

line widths. From his own observations and analysis, Beckman obtained 2.3 atmospheres for the cloud top pressure. Owen and Mason, using the line widths measured by Spinrad and Trafton (1963) and pressure broadening coefficients measured by Rank, Fink, and Wiggens (1966), obtained ≤ 1.6 atmospheres. They pointed out that if there is extensive multiple scattering just above the cloud layer, the derived pressure is likely to be too large; however, if the simple reflecting model is used to determine both the abundance and the pressure, a consistent set of values is obtained. If they had used this model to obtain the abundance of H_2, they would have obtained only 56 km-amagats rather than 85 km-amagats as found from the more sophisticated scattering model. Thus, according to their results, 56 km-amagats of H_2 lie above the level having a pressure of 1.6 atmospheres.

If one assumes that the difference between the total pressure and the partial pressure from the observed quantity of hydrogen is due to the partial pressure of helium, then the abundance of helium can be determined. The ratio of He to H_2 obtained in this way by Beckman is $\frac{3}{7}$ and by Owen and Mason, $\frac{2}{9}$.

A third technique by which to measure the abundance of He may prove profitable. It is the analysis of the limb darkening measurements made in the 8-14 μ region. Trafton (1967) has found that the limb darkening in this region, as given by Wildey (1964), can be explained in terms of absorptions due to H_2, He, and NH_3. However, models containing only H_2 and NH_3 are incompatible with the observations. I hope to

redo these calculations in the near future using the Rosseland mean opacities which I calculate in the second chapter and a new (supposedly better) limb darkening curve to be published by Wildey (see Wildey (1968)).

1.3 Temperature

Observations dealing with the temperature of Jupiter refer to two basically different types of measurements: brightness temperature, and the actual temperature of some particular level in the atmosphere.

a) Brightness Temperature

The brightness or radiometric temperature of a body is the temperature of a black body having the same surface brightness at a given wavelength as the given body does. Radiation reflected from or due to nonthermal sources should not be included in the measurement of the surface brightness. The effective temperature is an average brightness temperature--the temperature of a black body having the same flux or energy output per unit area as the body in question. It is this temperature which is the measure of the total energy balance of the planet. Unfortunately, the earth's atmosphere is opaque in many spectral regions, and so, at present, the observations of the brightness temperature of any body can be made only through the windows. The effective temperature must be estimated from the brightness temperatures.

Recent infrared measurements of Jupiter's brightness temperature are given in Table 1.2. The microwave spectrum is also a measure-

ment of the brightness temperature and these measurements have been listed separately in Table 4.2 p. 72

Table 1.2

Recent Measurements of
Jupiter's Brightness Temperature

Wavelength (μ)	Brightness Temperature (^{o}K)	Reference	Remarks
5	200±10	Low and Davidson (1968)	
10	125-132	Low and Davidson (1968)	appears to be variable
8-14	127	Wildey (1968)	includes isopotes
17.5-25	150±5 equator 130 poles	Low (1966)	
22	120-150	Low and Davidson (1968)	appears to be variable
1000-1400	153±15	Low (1965)	

Only Low and Davidson (1968) have observations at enough wavelenghts to reasonably estimate the effective temperature. They find the value to be 134±4^{o}K. The effective temperature has been theoretically calculated to be 104±3^{o}K from measurements of the albedo, under the assumption that the sun is the sole source of energy (see Section 4.1). If both of these values are correct, then the difference must arise from an internal heat source about twice as strong as that obtained from the sun.

It has generally been thought that any primordial heat that Jupiter may have had would have long since escaped. However, Hubbard (1968) concluded that the thermal conductivity of molecular

hydrogen has been greatly overestimated and that the cooling time for Jupiter is about 7×10^9 years. Then again, recent calculations by Bishop and DeMarcus (1968) have indicated that the cooling time is less than 10^9 years. Thus the issue is far from settled.

b) Temperature of Cloud Layer

A number of attempts have been made to determine the temperature of the cloud layer. In 1952 Kuiper (1952) calculated that the temperature of the cloud tops is at least 165-168°K, based upon the observed abundance of ammonia and the amount allowed by its vapor pressure. Owen and Woodman (1968) have used an analysis of the Jovian $3\upsilon_3$ band of methane at 11057Å to determine a rotational temperature of 180 ± 20°K. It is quite possible that the level in the atmosphere to which this value refers is somewhat deeper than for the temperature determined by Kuiper since the longer wavelength radiation used in the analysis by Owen and Woodman would not be so readily scattered. Danielson (1966), from an analysis of the Jovian collision induced 1-0 band of H_2 at 2.25μ found a temperature of about 250°K. However, on account of the absence of the strong H_2O bands at 1.9 and 2.7μ, he felt that the true temperature for the reflecting level at this wavelength is probably closer to 200°K.

1.4 Model Atmospheres

a) General

To make any significant progress in the type of analysis

discussed above, and to connect the various types of observations into a consistent picture, one must use a more detailed model atmosphere than has generally been used. Strictly speaking, a model is specified by its composition, internal and external energy sources, and the various interactions that can occur between these elements. The results of such a model are the equilibrium values of pressure, temperature and other variables of physical structure as a function of height. Temporal variations are generally left to the realm of meteorology. Except for condensables such as NH_3 and H_2O such variations are normally less than 10% of the average.

b) Models Previously Used

Model atmospheres for Jupiter have been calculated by Kuiper (1952), Öpik (1962), Lasker (1963), Gross and Rasool (1964) and Trafton (1967). Kuiper assumed, on the basis of the observed turbulence in the clouds, that the lower atmosphere was in convective equilibrium. Above the convective zone he placed an isothermal stratosphere at a temperature which would be appropriate for the case of Jupiter having no internal heat source. The temperature of the cloud top was obtained from the observed amount of NH_3 and the assumption that NH_3 was entirely saturated above the clouds. The pressure had to be determined from the observed amount of CH_4 and an assumed ratio of C/H. Altogether the approach was quite sound except for the determination of pressure which depended on rather shaky assumptions.

Lasker's main contribution was to determine the thermodynamic effects of the sublimation of ammonia on the adiabatic gradient. Öpik's work is a bit of an enigma. He attempted to derive a good model atmosphere for Jupiter by utilizing every facet of Jovian observations. In spite of his grand intentions, and although some of his work is brilliant, such as his analysis of the differences in contrast between the zones and the bands, Öpik drew some very unrealistic conclusions especially in regard to the composition of the atmosphere where he concluded that it contained over 97% helium. Gross and Rasool based their very approximate models on the assumptions that the atmosphere above the visible cloud layer is in radiative equilibrium and that NH_3 and CH_4 are the only sources of opacity. Trafton's models represent a tremendous improvement over all previous models. His were the first models which used molecular hydrogen as the source of opacity to thermal radiation. Also his models were the first to include the possibility of both radiative and convective equilibrium. A more complete description of his models and my improvements upon them is given in Section 2.1.

c) Effect of Clouds

Except for Öpik's work on the zones and bands, the actual structure of the clouds has been, for the most part, ignored in the models described above. Trafton concluded that there should be a thin haze of particles of solid ammonia lying above the convection zone. This haze would be generated by the very slight upset from hydrostatic

equilibrium caused by the condensation of ammonia, which, in turn, would cause a very slow mixing of the atmosphere above the main clouds.

The observed reduction in the strengths of the CH_4 and NH_3 absorption lines near the limbs of the planet (Hess (1953), Münch and Younkin (1964), and Teifel (1966)) have led Hess to conclude that the cloud layer must be higher in the atmosphere in the Jovian morning and evening than it is at noon. Squires (1957) argued against the changing cloud height hypothesis, and instead showed that a cumuliform cloud structure would not only be more likely, but could also explain the center to limb variations in line strength. According to Owen and Mason (1968) these same variations can also be explained by a strongly scattering atmosphere.

1.5 Models for the Radio Brightness Temperature

An early attempt to explain the Jovian microwave radiation was made by Field (1959). He calculated the expected thermal emission at decimeter wavelengths that would be obtained with ammonia supplying the opacity. The calculations were performed with the use of the single line approximation in which it is assumed that the absorption from all the NH_3 inversion lines can be suitably represented by a single line of the same total intensity as the real lines and with an average central frequency and line width. A simple convective model atmosphere was used. One of the conclusions of this work is that the radiation at these wavelengths is of mostly nonthermal origin.

Winter (1964) also used the single line approximation with convective model atmospheres to calculate the expected emission temperature from Jupiter for wavelengths near 1 cm. He found that the shape of the dip in the brightness temperature of Jupiter, that occurs at the ammonia inversion frequency, varied significantly with the assumed cloud top pressure. Naumov and Khizhnyakov (1965) calculated the absorption coefficient of ammonia much more accurately than did the previous investigators. However, they coupled this to ridiculous model atmospheres, which assumed that the clouds radiated like a black body at 130°K. Consequently their results are quite invalid. Law and Staelin (1968) calculated the brightness spectrum of Jupiter using the 66 ammonia lines tabulated in Townes and Schawlow (1955) and a number of Kuiper-type model atmospheres. Their results are in basic agreement with the observations. However, more detailed model atmospheres must be used if one hopes to use the microwave observations to learn anything new about the atmospheric structure of Jupiter.

1.6 Scope of Thesis Research

Trafton's model atmospheres were used as a basis for making "improved" models as they were the most sophisticated and correctly took account of the major interactions. This thesis adds to his models the effect of the absorptions by ammonia and methane, effects which become increasingly important as the effective temperature of the model is increased. Chapter 2 contains the discussion of the thermal

opacities of NH_3 and CH_4 and the quantitative way in which they modify Trafton's models. The microwave absorption coefficient including the absorption by hydrogen molecules is discussed in Chapter 3. In Chapter 4 the models and the absorption coefficient obtained from the two preceding chapters are used to obtain the radio brightness temperature. The conclusions which can be drawn from a comparison of the observed microwave spectrum with theoretical spectra and from other characteristics of the models will be found in Chapter 5. It was hoped that these comparisons of the microwave spectrum would allow a better determination of Jupiter's composition and effective temperature, one that was independent of the confusing effects caused by the cloud structure. The success of this phase of the research has been limited to a large extent by the large errors associated with the observations. The appendices contain details of the microwave absorption coefficients of ammonia and of water.

2. Construction of the Models

2.1 General

The models of the Jovian atmosphere calculated in this thesis are an extension of the models computed by Trafton (1965, 1966b, 1967, 1968). Trafton computed the variation of temperature and pressure with depth in the Jovian atmosphere under the following assumptions:

1. The upper atmosphere is in a state of radiative equilibrium.
2. The thermal opacity is due to pressure-induced dipole absorption by H_2 and its enhancement in mixtures containing He.
3. Scattering of thermal radiation is negligible.
4. The flux is constant throughout the radiative portion of the atmosphere and is entirely in the radial direction.
5. The unsaturated components of the atmosphere are uniformly mixed.
6. The atmosphere is in hydrostatic equilibrium.
7. The population of the energy levels corresponds to local thermodynamic equilibrium.
8. The depth at which convection sets in was found by comparing the radiative gradient with the wet adiabatic

gradient, which includes effects due to saturated atmospheric components.

The models are specified by their effective temperature and composition. The effective temperature, T_e, is a measure of the radiative flux, $\mathcal{F}$, through the relationship $\mathcal{F} = \sigma T_e^4$. The composition is given in terms of the fractional abundance or mixing ratio of each unsaturated component. α_1, α_2, α_3, α_4, and α_5 are the mixing ratios of H_2, He, NH_3, H_2O, and CH_4 respectively. Both NH_3 and H_2O become saturated in some region of the atmosphere.

The initial Te=110°, 120°, and 130° -models were obtained directly from Trafton's calculations, but the 140° -model was obtained from a homology transformation applied to the 130° -model (see Section 2.2 on next page).

I have modified Trafton's initial models to include, in an approximate manner, the additional absorption by ammonia and methane. The result of this modification is an increase in the radiative gradient and a raising of the level at which convection begins.

The conditions in the convective region of the atmosphere were computed using Trafton's (1967) equations for the wet adiabatic gradient, but also including water as a saturable component. Even though water has not been observed in the Jovian atmosphere, it is likely to exist at levels below the cloud layer and may cause an

observable effect on long wavelength radiation, which arises from much greater depths than the tops of the visible clouds.

The techniques and equations used are given in the following sections of this chapter.

2.2. Homology Transformation

According to Trafton (1965) his $\alpha_2 = 0$ -models are approximately homologous with the following transformations:

$$P = g^{\frac{1}{2}}\mu^{\frac{1}{2}}T_o^{\frac{1}{2}}\alpha_1^{-1}\underline{P},$$

$$x = g^{-1}\mu^{-1}T_o\underline{x}, \quad \text{and} \tag{2.1}$$

$$T = T_o\underline{T}$$

where P, x, and T are the pressure, depth, and temperature respectively, $\underline{P}$, $\underline{x}$, and $\underline{T}$ are the corresponding non-dimensional transformed variables defined by the above equations, and g, μ, and T_o are the gravitational acceleration, mean molecular weight, and the stratospheric temperature respectively.

If transformations are made only between Jovian models with the same composition, g, μ, and α_1 can be regarded as constants and the transformation equations can be written:

$$\frac{P_2}{P_1} = \left(\frac{T_{o2}}{T_{o1}}\right)^{\frac{1}{2}}, \quad \frac{\dot{x}_2}{\dot{x}_1} = \frac{T_{o2}}{T_{o1}}, \text{ and } \frac{T_2}{T_1} = \frac{T_{o2}}{T_{o1}} \qquad (2.2)$$

where the subscripts 1 and 2 represent the parameters for a given model and an homologous model. A variation on equations 2.2 when applied to the 110° -model to predict the 120° -model, and when applied to the 120° -model to predict the 130° -model was empirically found to match Trafton's models more accurately than predictions based on equations 2.2. Models based on the modified equations were within .001 in log P, .3km in x, and $.3^{\circ}K$ in T of Trafton's models in the radiative regions of the atmosphere. The modified equations used in place of equations 2.2 are:

$$\frac{P_2}{P_1} = \left(\frac{T_{o2}}{T_{o1}}\right)^{1/2.9}, \quad \frac{\dot{x}_2}{\dot{x}_1} = \frac{T_{o2}}{T_{o1}}, \text{ and } \frac{T_2}{T_1} = \left(\frac{T_{o2}}{T_{o1}}\right)\left(\frac{T_1}{T_{o1}}\right)^{.0029(T_{o2}-T_{o1})} \qquad (2.3)$$

The last equation is not of the proper mathematical form to represent a general transformation between models of different effective temperatures as it is not associative, i.e. two successive transformations $T_{o1} \rightarrow T_{o2}$ and $T_{o2} \rightarrow T_{o3}$ are not equivalent to the single transformation $T_{o1} \rightarrow T_{o3}$. However for any realistic case the error is negligible.

For Trafton's 110°, 120°, and 130° -models there is an $8^{\circ}K$ difference in T_o for a $10^{\circ}K$ difference in Te. The constant .0029 in

equation 2.3 was chosen to give the best fit for transformations in which $T_{o2} - T_{o1} = 8^{o}K$. The 140^{o} -model was computed from equations 2.3 using the 130^{o} -model as the initial model with $T_{o2} = 109.6^{o}K$, which is $8^{o}K$ higher than the stratospheric temperature of the 130^{o} -model.

The transformation for the radiative gradient can be obtained from equations 2.2 or 2.3 depending on which set of transformations are employed. For equations 2.2 and 2.3 one has respectively:

$$\left(\frac{d\ln T}{d\ln P}\right)_2 = \left(\frac{d\ln T}{d\ln P}\right)_1 \quad \text{and} \tag{2.4}$$

$$\left(\frac{d\ln T}{d\ln P}\right)_2 = [1 + .0029(T_{o2}-T_{o1})]\left(\frac{d\ln T}{d\ln P}\right)_1 . \tag{2.5}$$

2.3 Absorption Coefficients

In order to modify the radiative regions of Trafton's model atmospheres to include the effects of absorption of thermal radiation by ammonia and methane, the absorption coefficients of hydrogen, ammonia and methane are needed.

The absorption coefficient of hydrogen is continuous, that is, it is a smoothly varying function of frequency and therefore can be represented by a relatively small number of points. However the absorption from ammonia and methane is due to very many discrete lines which are often formed into bands of lines with the individual lines

more-or-less randomly spaced within the bands. An exact description of the absorption coefficients of these molecules cannot be calculated and would require better laboratory data than presently exist. The exact configuration is also far more than is required. What is needed is some sort of mean absorption coefficient averaged over a small frequency interval. The type of mean depends upon the particular problem at hand, and its value may be determined by the use of a model whereby the main features of the absorption coefficient can be described by a few easily-handled parameters. These parameters, in turn, may be determined through the application of an appropriate model to measured absorption curves.

a) Hydrogen

Trafton writes the absorption coefficient for hydrogen as

$$\kappa_\upsilon = \frac{1}{k^2 c}\left(\frac{P\alpha_1}{T}\right)^2 \left[A\upsilon + \frac{\alpha_2}{\alpha_1} B\upsilon\right] \qquad (2.6)$$

where κ_υ is the monochromatic absorption coefficient in cm^{-1}, and

$A\upsilon$ and $B\upsilon$ are his "absorption coefficients;"

$A\upsilon$ is due to H-H collisions and

$B\upsilon$ is due to He-H collisions.

Trafton has been kind enough to supply me with tabulated values of $A\upsilon$ and $B\upsilon$, which I have used in all succeeding computations. The equations used to compute $A\upsilon$ and $B\upsilon$ are given in his thesis.

b) Ammonia and Methane

Plass (1958, 1960) has described a number of models which may be used to represent absorption in molecular bands. He also gives techniques for determining the values of the band parameters from the measured absorption curves--a good determination requires a knowledge of how the absorption varies with pressure and quantity of absorber. Since the spectrum of ammonia contains many gaps between the bands of lines, an extension to these models has been made to represent the absorption in the gaps.

The lines are assumed to have the Lorentz line shape since, for Jovian conditions, Doppler broadening of the lines is negligible compared with pressure broadening.

i) Single Line Parameters

The absorption coefficient for a single line with a Lorentz shape is given by

$$\kappa_{sl} = \frac{SN_i}{\pi} \frac{\Delta\nu}{(\nu-\nu_o)^2 + \Delta\nu^2} \qquad (2.7)$$

where κ_{sl} is the absorption coefficient for a single line (cm^{-1}),

S is the line strength per molecule (cm),

N_i is the number density of absorbing molecules of the i^{th} type (cm^{-3}),

ν_o is the central frequency of the line (cm^{-1}), and

Δ_ν is the half width of the line (cm^{-1}).

The half width of a pressure broadened line is a function of the pressure, temperature, type of colliding molecule, and the transition giving rise to the line. The pressure and temperature dependence is expressed by equation A.15 with n=3 for collisions between NH_3 and NH_3, and n=7 for collisions between NH_3 and He, H_2, N_2, etc. If the strongest interaction between methane and other nonpolar molecules is the London dispersion force, then n=6 for collisions between CH_4 and He, H_2, N_2, etc. The actual half widths of the individual lines are seldom known, but it is convenient to give them in terms of their values under some standard conditions. Nitrogen has been taken as a standard broadening gas in measurements of spectra made in laboratories. Therefore I have taken as a standard, the line widths for a dilute mixture of absorbing gas in N_2 at STP. In terms of the line widths under the standard conditions, the widths for other conditions may be written:

$$\Delta\upsilon_{NH_3} = \left\{C_{NH_3}\left(\frac{P_{NH_3}}{760}\right)\left(\frac{273}{T}\right) + \sum_i C_i \left(\frac{P_i}{760}\right)\left(\frac{273}{T}\right)^{2/3}\right\}\Delta\upsilon_s \qquad (2.8)$$

$$\Delta\upsilon_{CH_4} = \left\{\sum_i C'_i \left(\frac{P_i}{760}\right)\left(\frac{273}{T}\right)^{7/10}\right\}\Delta\upsilon_s \qquad (2.9)$$

where C_i and C'_i are the broadening constants for gas i with ammonia and methane respectively. (For N_2 both of these constants have been defined to be 1.)

P_i is the partial pressure of gas i in mmHg, and

$\Delta\nu_s$ is the half width of the line under the standard conditions. The values of the C_i can be readily determined from the measured widths of NH_3 lines which were pressure broadened by various gases. This information is given in Townes and Schawlow, Table 13-4. The results are

$$C_{N_2} \equiv 1,\ C_{H_2} = 0.79,\ C_{He} = .34,\ C_{NH_3} = 7.3.$$

Since detailed measurements of the line widths of methane are not available, I have used the broadening coefficients for methane given by Burch, Singleton, and Williams (1962), and by France and Williams (1966). These coefficients are, in effect, the ratios of pressures of nitrogen to other gases for the same amount of broadening. An examination of equation 2.9 will show that these ratios are the same as the C_i's. The broadening coefficient for hydrogen on methane was not found, so the value for hydrogen on carbon-dioxide was used in its place since the helium and argon broadening coefficients on carbon-dioxide are about the same as on methane. The values I have used are:

$$C'_{N_2} \equiv 1,\ C'_{H_2} = 1.17,\ C'_{He} = 0.56,\ C'_{CH_4} = 1.38.$$

A knowledge of the approximate widths of the spectral lines of ammonia and methane has facilitated the analysis of the structures of

the bands. An approximate average value for the half-widths of the ammonia lines can be obtained from equation A.16a with $K = \frac{1}{2}J$ and $J(J+L) \sim J^2$. For methane I have used the half-width of the single line which was measured by Sakurai and Shimoda (1961). These widths have been converted to their values at the standard conditions through equations 2.8 and 2.9. The results are

$$\Delta\nu_s(NH_3) \approx 0.070 \text{ cm}^{-1}, \quad \Delta\nu_s(CH_4) \approx 0.175 \text{ cm}^{-1} \quad (2.10)$$

As may be seen from an inspection of equation A.5, S in equation 2.7 is a function of temperature through the relationship

$$S \propto f(1-e^{-\frac{hc\nu}{kT}}) \quad (2.11)$$

where f is the fraction of molecules in the level from which the line originates, and

the factor in parentheses accounts for stimulated emission. The functional dependence of f on temperature for ammonia, as given by equation A.13 is

$$f(T) \propto \left(\frac{1}{T}\right)^{3/2} e^{-E/kT} \quad (2.12)$$

where for lines originating in the ground vibrational level, E is given by equation A.1, and for lines originating from excited vibrational levels E has been claculated by Garing, Nielsen, and Rao (1959).

Methane is a spherical top molecule which means that the moments of inertia around any three perpendicular axes are equal. For such a molecule the formulae for the energy levels and for the partition function (aside from a constant factor) are given by equations A.1 and A.11 with A = B. Thus the functional form of f(T) is the same for methane as it is for ammonia. Herzberg (1945) gives the rotational constant of methane as

$$B = 5.25 \text{ cm}^{-1} . \qquad (2.13)$$

Because of the symmetry of the methane molecule there is no pure rotational spectrum. The lowest frequency transitions for which strong absorption occurs are in the vibrational-rotational band $\nu_4 \leftarrow 0$, centered at 1306 cm^{-1}. There are no other strong bands in the frequency region which I have considered.

Although equation 2.11 is accurate for a single line it is only approximate when applied to a band as a whole because each line in a band originates at a slightly different energy level. Because of this uncertainty I have expressed S at other temperatures in terms of its value, S_s, at 300°K--approximately the temperature at which the labora-

tory spectra were obtained. The relationship is

$$S = \left(\frac{300}{T}\right)^{3/2} \exp\left(\frac{E}{k300} - \frac{E}{kT}\right) \frac{1-\exp(-\frac{hc\nu}{kT})}{1-\exp(-\frac{hc\nu}{k300})} S_s \qquad (2.14)$$

Another parameter in equation 2.7 which depends upon the physical conditions in the atmosphere is the number density of absorbing molecules, N_i. I have chosen to write N_i in terms of its value at S.T.P.:

$$N_i = \left(\frac{P_i}{760}\right)\left(\frac{273}{T}\right) L_o \qquad (2.15)$$

where L_o is Loschmidt's number.

The partial pressures of methane and ammonia when ammonia is not saturated are given by the products of their respective mixing ratios and the total pressure. When the pressure for ammonia computed in this manner exceeds the vapor pressure of ammonia (equation 2.36) ammonia is saturated, in which case I have assumed that its partial pressure is equal to its vapor pressure.

ii) Band Parameters

In the analysis, I have used two of the models described by Plass (1958)--the Elsasser model of a band and the statistical models of a band. An Elsasser band is composed of uniformly spaced identical spectral lines, each having a Lorentz line shape. The statistical model that I have used is similar except that the lines are randomly spaced. The line spacing in a real band falls someplace between these

two cases. The predicted absorption, as a function of pressure and quantity of absorber is about the same for both models except when the absorption is high. Trafton has done some analysis of the ammonia bands using the statistical model, and for the sake of compatibility, I have done likewise. (However, agreement between my results and his is purely qualitative.)

The same notation will be used for both models: all lines in a band have strength S, half width $\Delta\nu$, and have an average separation from each other d. A gap has width $2\delta d$ and is bordered on both sides by similar bands. $f\delta d$ is the frequency difference from a point in a gap to the edge of a bordering band. In a frequency interval containing a number of bands and gaps, p is the fraction of that interval occupied by bands, and (1-p) is the fraction occupied by gaps. This notation is further illustrated, for the case of the Elsasser band model, in Figure 2.1

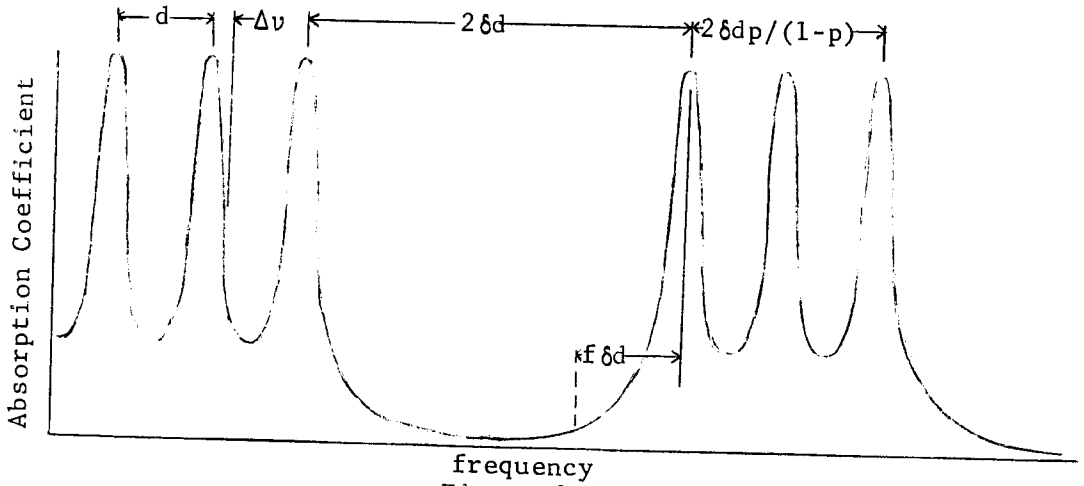

Figure 2.1

Schematic Absorption Coefficient for Band and Gap Model

Plass has quite thoroughly described the absorption predicted by various band models. I shall list only the most general conclusions here. For the two band models which I have considered, the absorption can be expressed as a function of two parameters:

$$\beta = \frac{2\pi\Delta\nu}{d} \quad \text{and} \quad xL = \frac{SN_i}{2\pi\Delta\nu}L \tag{2.16}$$

where L is the path length of the radiation through the gas in cm. (Plass' x is the same as my xL.) When the peaks of the individual spectral lines are highly saturated, as is usually the case in laboratory spectra, the absorption is a function of the single term $\beta^2 xL$. When the lines are weak even at their centers, the absorption is a function of the term βxL.

Thus it is not always possible to determine β or x separately from laboratory absorption curves made over a limited range of conditions. Sometimes additional information is available from high resolution spectra. I have attempted to minimize the effect of the mixing of data of different types by using $\beta^2 x$ and β as the band parameters. β is directly proportional to $\Delta\nu$. Therefore its dependence on P and T is the same as is $\Delta\nu$'s, i.e. equation 2.8 or 2.9. $\beta^2 x$ is directly proportional to $SN_i\Delta\nu$ so its dependence on P and T is given by the product of equations 2.14, 2.15, and 2.8 or 2.9.

The absorption in the gaps must also be taken into account. The absorption coefficient within a gap can be written as the sum of

the absorption coefficients in the wings of the lines belonging to the bands on either side of the gap:

$$\kappa_{\nu g} = \frac{SN_i}{\pi} \sum_{n=0}^{\infty} \left(\frac{\Delta\nu}{(f\delta d+nd)^2+\Delta\nu^2} + \frac{\Delta\nu}{(2\delta d-f\delta d+nd)^2+\Delta\nu^2} \right) \quad (2.17)$$

where I have used the Elsasser model to represent the bands.

For regions far enough from the gap's edges such that the $\Delta\nu^2$ terms in the denominators of equation 2.17 can be ignored, the summation has been performed by following a technique described in the Handbook of Mathematical Functions (1964), page 264. The result is

$$\kappa_{\nu g} \approx \frac{1}{2\pi^2} \beta^2 x \left[\psi(f\delta)+\psi(2\delta-f\delta)\right] \quad (2.18)$$

where $\psi(x)$ is the digamma function and is defined by $\psi(x) \equiv \frac{d^2}{dx^2} \ln\Gamma(x)$, and the value of $\beta^2 x$ is the same as used for the surrounding bands.

Thus at the center of the gap the absorption is $A \approx 1-\exp(-\beta^2 x \frac{\psi(\delta)}{\pi^2})$.

An asymtotic expression for $\psi(x)$ is

$$\psi(x) \approx \frac{1}{x} + \frac{1}{2x^2} + \frac{1}{6x^3} - \frac{1}{30x^5} + \cdots \quad (2.19)$$

For mathematical simplicity I have kept only the first term in equation 2.19. Since δ is usually much greater than 1, this is a suitable

approximation over most of the gap.

The sources I have used in obtaining the absorption coefficient of ammonia are France and Williams (1966), Owen and Walsh (1965), Loewenstein (1960), Garing, Nielsen, and Rao (1959), Mould, Price and Wilkinson (1959), American Petroleum Institute Research Project 44 Serial No. 1713 (1955), Foley and Randall (1941), Wright and Randall (1933), and Badger and Cartwright (1929). For methane the sources I have used are Burch and Williams (1962), American Petroleum Research Project 44, Serial No. 528 (1946), and Nielsen and Nielsen (1935).

The spectra which were measured generally fell into one of two groups: 1. low resolution spectra with only the bands and gaps resolved and showing the variation of absorptance with pressure and quantity of absorber, and 2. high resolution spectra with almost all of the individual lines resolved but usually having poor intensity calibration. For spectra of the first type a plot of the absorptance versus the product of the pressure and the quantity of absorber will show for which conditions the lines are saturated and for which conditions they are weak. The appropriate equations, Plass (1960) equations 8 or 12, were then used to determine the band parameters $\beta^2 xL$ or βxL from the absorptance. For spectra of the second type the equivalent widths and spacing of typical lines in a band were measured. Since the cores of these lines were saturated, the parameters $\beta^2 xL$ were determined from Plass (1958) equation 8, and the parameters β from equation 2.10 and the measured

line spacing. The values of $\beta^2 x$ and β thus determined have been reduced to their values under the standard conditions by use of the relations described on page 30.

I have not given the details of the analysis as the method differed depending upon the nature and detail of the spectral information given each source. Often, a lot of judgment had to be used rather than straight "cookbook" procedure.

Tables 2.1 and 2.2 give the results of this analysis for the band parameters of ammonia and of methane respectively. In Column 1 are listed the frequencies at which the band parameters were determined. Columns 2 and 3 contain the quantities $(\beta^2 x)_s \equiv \frac{S_s L_o}{d} \frac{2\pi\Delta\nu_s}{d}$ cm^{-1} and $\beta_s \equiv \frac{2\pi\Delta\nu_s}{d}$ respectively. Column 4 contains the approximate average value of the energies of the lower levels of the transitions giving rise to the spectral lines. The units of energy are cm^{-1}. In column 5 are given the values of δ for those cases in which gaps do exist between bands of lines. Column 6 contains the values of p, the average fraction of a frequency interval occupied by bands.

In use these parameters have been converted to their values at the conditions which exist in the Jovian atmosphere, again by the procedure described on page 30.

Table 2.1

Parameters for the Absorption Coefficient of Ammonia

ν (cm^{-1})	$(\beta^2 x)_s$ (cm^{-1})	β_s	E (cm^{-1})	δ	p	ν (cm^{-1})	$(\beta^2 x)_s$ (cm^{-1})	β_s	E (cm^{-1})	δ	p
32	.1+	.73	15	17	.03	520	6.8×10^{-4}	.18	1350	---	1
64	.62	.28	60	5.9	.08	553	4.7×10^{-3}	.27	1135	4.7	.24
96	3.5	.46	166	9.5	.09	587	1.1×10^{-2}	.43	1050	8.8	.05
128	6.0	2.1	310	43	.11	638	1.0×10^{-2}	.91	1350	---	1
161	7.6	2.3	470	43	.13	690	8.8×10^{-3}	.21	1000	---	1
193	2.6	1.9	650	35	.19	741	.15	.74	1140	---	1
225	1.2+	1.5	900	25	.26	793	.18	.56	470	---	1
257	.46+	1.4	1200	19	.36	845	.53	.25	250	2.0	.35
289	.24+	1.1	1500	12	.48	896	.46	.25	100	1.9	.21
322	.11	.9+	1885	7+	.6+	948	5.74	.55	213*	--	1
354	1.0×10^{-2}	.69+	2100+	---	1	999	.76	.30	56	3.0	.49
387	3.9×10^{-3}	.53+	1900	---	1	1124	9.8×10^{-2}	.14	524	---	1
420	3.2×10^{-3}	.40+	1700+	---	1	1250	9.3×10^{-4}	.61	1560	---	1
454	2.8×10^{-3}	.31+	1640+	---	1	1374	1.7×10^{-3}+	.7+	760	---	1
487	3.9×10^{-3}	.24+	1450+	---	1	1499	.32	.84	585	---	1

+ estimated value

*The absorption near this frequency is due to transitions arising from all J levels, thus f (eqs. 2.11 and 2.12) is independent of temperature. E = 213 cm^{-1} is an effective value for use in eq. 2.12 to cause $f(150^o) = f(300^o)$.

Table 2.2

Parameters for the Absorption Coefficient of Methane

υ (cm^{-1})	$(\beta^2 x)_s$ (cm^{-1})	β_s	E (cm^{-1})	δ	p
1124	0	---	---	---	0
1250	.39	2.9+	420	---	1
1374	.28	2.5+	820	---	1
1499	0	---	---	---	0

+estimated value

c) Mean Absorption Coefficient

As was mentioned earlier, what is needed is some sort of mean absorption coefficient averaged over a small frequency interval. As will be explained in the next section of this chapter, the average which is appropriate for the determination of the radiative gradient is the harmonic mean of the sum of the absorption coefficients of each constituent. Unfortunately this average cannot be related exactly to any average for each component separately. For example, if the absorption by ammonia is everywhere greater than the absorption by hydrogen, the harmonic mean of the ammonia absorption coefficient is appropriate, but if it is everywhere less, the straight mean is appropriate. Since the hydrogen absorption coefficient is relatively smooth over a small

frequency interval, it can be represented by a constant value. Then, letting $\langle\ \rangle$ represent the harmonic mean, the harmonic mean of the sum of a continuous absorption coefficient such as κ_{H_2} and one composed of bands and gaps such as κ_{NH_3} can be written

$$\langle \kappa \rangle = \kappa_{H_2} \left\langle 1 + \frac{\kappa_{NH_3}}{\kappa_{H_2}} \right\rangle \equiv \kappa_{H_2} (1 + R_{NH_3}). \qquad (2.20)$$

The product $\kappa_{H_2} R_{NH_3}$ can be thought of as the effective ammonia absorption coefficient. There is no significant overlapping of the absorption by methane with that by ammonia; therefore when both ammonia and methane are included, equation 2.20 can be written

$$\langle \kappa \rangle = \kappa_{H_2} (1 + R_{NH_3} + R_{CH_4}). \qquad (2.21)$$

The quantity R can be evaluated by using a model for the ammonia or methane absorption coefficient. Since the statistical model was used to evaluate the band parameters from the laboratory spectrograms, it would seem only natural to use this same model to evaluate R. However mathematical difficulties precluded this possibility so I used the Elsasser band model. The absorption coefficient in an Elsasser band is given by

$$\kappa_{\nu b} = \beta x\left(\frac{\sinh\beta}{\cosh\beta-\cos\theta}\right) = \beta^2 x\left(\frac{\tanh\beta}{\beta}\right)\left(\frac{\cosh\beta}{\cosh\beta-\cos\theta}\right) \qquad (2.22)$$

where $\theta = \frac{2\pi(\nu-\nu_o)}{d}$, and

ν_o is the central frequency of a line in the band.

In a gap the absorption coefficient is given by equation 2.18.

From equation 2.20 and 2.22, and 2.18 and from the definition of harmonic mean it can be shown that

$$R_{NH_3} = \left\langle 1+\frac{\kappa_{NH_3}}{\kappa_{H_2}}\right\rangle -1$$

$$= \left\{p\frac{1}{\pi}\int_o^{\pi}\left(1+\frac{\kappa_{\nu b}}{\kappa_{H_2}}\right)^{-1} d\theta+(1-p)\int_o^{1}\left(1+\frac{\kappa_{\nu g}}{\kappa_{H_2}}\right)^{-1} df\right\}^{-1} -1 \qquad (2.23)$$

$$= \left\{1-\frac{pu}{\left[u^2+2u+\tanh^2\beta\right]^{\frac{1}{2}}} - \frac{(1-p)v}{2\left[1+v\right]^{\frac{1}{2}}}\ln\left(\frac{\sqrt{1+v}+1}{\sqrt{1+v}-1}\right)\right\}^{-1} -1$$

where $u = \frac{\beta^2 x}{\kappa_{H_2}}\frac{\tanh\beta}{\beta}$, and $v = \frac{1}{\pi^2\delta}\frac{\beta^2 x}{\kappa_{H_2}}$.

Equation 2.23, of course, also applies to methane.

2.4 Radiative Gradient

Trafton's radiative solutions for the atmospheres of the Jovian planets are based upon the assumption that hydrogen is the only significant absorber of thermal radiation in these planets. This assumption

appears to be quite good for Saturn, Uranus, and Neptune as these planets are so cold that ammonia is almost entirely frozen out and there is extremely little radiation of a high enough frequency to be absorbed by methane. For Jupiter, hydrogen is still the major absorber, but absorption by ammonia and methane is significant--especially for models with a high effective temperature.

The hydrostatic equilibrium equation can be combined with the perfect gas law to give for the temperature gradient

$$\frac{d\ln T}{d\ln P} = \frac{R}{\mu g}\left(\frac{dT}{d\tau_s}\right)\kappa_s \qquad (2.24)$$

where κ_s is the absorption coefficient in cm^{-1} at some standard frequency, and

τ_s is the total optical depth at that same frequency.

Trafton properly carried out the computation of $\frac{dT}{d\tau_s}$ for his models. But the procedure for doing so is quite complex, so I have resorted to what at first might appear as a rather crude approximation in order to determine the manner in which the radiative gradient depends upon the absorption coefficient. With this I will, utilizing a perturbation procedure, calculate a corrected value for Trafton's radiative gradients which includes the effects of absorption by ammonia and methane.

Schwarzschild (1958) gives an approximate equation for the radiative flux at a point in the atmosphere

$$\mathcal{F} = \frac{4}{3\bar{\kappa}} \frac{d}{dx} (\sigma T^4) = \frac{16\sigma}{3} \frac{\kappa_s}{\bar{\kappa}} T^3 \left(\frac{dT}{d\tau_s}\right) \qquad (2.25)$$

where $\mathcal{F}$ is the radiative flux, and

$\bar{\kappa}$ is the flux-weighted mean absorption coefficient in cm^{-1}.

Equations 2.24 and 2.25 can be combined to give

$$\frac{d\ln T}{d\ln P} = \frac{3}{16} \frac{RT}{\mu g} \frac{\mathcal{F}}{\sigma T^4} \bar{\kappa} \; . \qquad (2.26)$$

For an atmosphere in radiative equilibrium $\mathcal{F} = \sigma Te^4$ and the gradient $\frac{d\ln T}{d\ln P}$ is the radiative gradient $\left.\frac{d\ln T}{d\ln P}\right|_{RAD} \equiv G_R$. Thus for a region which is in radiative equilibrium, equation 2.26 becomes

$$G_R = \frac{3}{16} \frac{RT}{\mu g} \left(\frac{Te^4}{T^4}\right) \bar{\kappa} \; . \qquad (2.27)$$

An approximate expression for $\bar{\kappa}$ is the Rosseland mean opacity:

$$\frac{1}{\bar{\kappa}} = \frac{\int_0^\infty \frac{1}{\kappa_\upsilon} \frac{dB_\upsilon}{dT} d\upsilon}{\int_0^\infty \frac{dB_\upsilon}{dT} d\upsilon} \; . \qquad (2.28)$$

Equation 2.25 requires the approximation that the intensity can be

written $I = I_o + I_1 \cos\theta$, and equation 2.28 requires the assumptions that $\frac{dT}{d\tau} \lll \frac{1}{8}T$ and $\frac{dT}{d\tau}$ is constant from about τ-2 to τ+2. In the region of the atmosphere presently being considered, where the optical depth is not far from one, these conditions are not met. However, when all is said and done, the proof is still in the pudding.

Using equation 2.27 and the absorption coefficient for hydrogen and helium given by equation 2.6 I have computed the radiative gradient for all of Trafton's models. The upper limit of integration in the numerator of equation 2.28 was taken to be $1499 cm^{-1}$. This is equivalent to assuming complete absorption at higher frequencies. Trafton made a similar assumption on the grounds that there is strong absorption by ammonia and methane near that frequency. Radiative gradients calculated in this manner approach Trafton's more accurately calculated values in the deeper levels of the atmosphere and are within 8% of his at the top of the convective region. Although equation 2.27 is not quite accurate enough to refine the value of the radiative gradient when ammonia and methane are added as absorbers, it is accurate enough to give one a reasonable degree of confidence as to the functional dependence of the radiative gradient on the absorption coefficient: the radiative gradient is directly proportional to the Rosseland mean opacity.

With the inclusion of ammonia, κ_ν is a much more rapidly varying function of frequency than is $\frac{dB_\nu}{dT}$. The integral in the numerator of equation 2.28 can be divided up into integrals over frequency regions

small enough so that $\frac{dB_\nu}{dT}$ is essentially constant over the interval. Thus

$$\int_{\Delta\nu} \frac{1}{\kappa_\nu} \frac{dB_\nu}{dT} d\nu \approx \frac{dB_\nu}{dT} \int_{\Delta\nu} \frac{1}{\kappa_\nu} d\nu = \frac{dB_\nu}{dT} \langle \frac{1}{\kappa_\nu} \rangle \Delta\nu \qquad (2.29)$$

where $\langle \kappa_\nu \rangle$ is the harmonic mean value of κ_ν over the interval. Since the integration in equation 2.28 must actually be performed through the summation of terms of the form shown in equation 2.29, an average value of κ_ν must be used, and, as just shown, the appropriate average is the harmonic mean of the sum of the absorption coefficients of each constituent.

Thus a first approximation for the corrected value of the radiative gradient can be found by multiplying Trafton's value by the ratio of the Rosseland mean opacity including absorption by H_2, He, NH_3 and CH_4 to the value obtained using absorption by only H_2 and He. An additional correction must still be applied since a corrected value for the gradient will result in a change in the pressure, and this, in turn, will result in a change in the absorption coefficient. Both of these may be taken into account in the following manner. The additional absorption by ammonia and methane is small compared with that by hydrogen and helium, and thus, from equation 2.6, the absorption coefficient is approximately proportional to the square of the pressure. With this approximation, the equation for the radiative gradient is

$$\frac{G_R}{G_o} = \frac{\kappa_1}{\kappa_o}\left(\frac{P}{P_o}\right)^2 \qquad (2.30)$$

where $$G_R = \frac{d\ln T}{d\ln P},\ G_o = \frac{d\ln T}{d\ln P_o}\ , \qquad (2.31)$$

and where the subscript "o" stands for the values in Trafton's models; κ_o is the Rosseland mean opacity including only H_2 and He, evaluated at a temperature T and pressure P_o; κ_1 is the Rosseland mean including H_2, He, NH_3 and CH_4 evaluated for the same conditions as for κ_o; and P is the corrected value of the pressure at temperature T.

Equations 2.30 and 2.31 can be solved for the pressure:

$$P = \left[\int_o^{P_o} \frac{\kappa_o}{\kappa_1}\, dP_o^{\,2}\right]^{\frac{1}{2}}. \qquad (2.32)$$

The depth, x, associated with temperature T must also be corrected. Using equations 2.24 with $\kappa_s = \frac{d\tau_s}{dx}$ and 2.31 one has

$$\frac{dT}{dx} = \frac{\mu g}{R} G_R \quad \text{or} \quad \frac{dx_o}{dx} = \frac{G_R}{G_o} \qquad (2.33a\ \&\ b)$$

Either of equations 2.33 can be integrated to find the depth.

In the calculation of κ_1 I have assumed that the mixing ratio for methane $\alpha_5 = .003$ in all models. This value was chosen as it is compatible with the observed ratio of methane to hydrogen in the Jovian

atmosphere. Reasonable variations in α_5 are not expected to cause any significant variation in $\varkappa_1$.

The values for G_o were obtained as follows. For the pure-hydrogen models the values given in Trafton's computer output for his $\frac{\alpha_2}{\alpha_1} = 0$, Te = 120°K model were used after being modified by the homology transformation equation 2.5 to make them applicable to models of other effective temperatures. For the models containing 50% helium, no significant dependence of the gradient on effective temperature was evident in Trafton's results, so the values given for the $\frac{\alpha_2}{\alpha_1} = 1$, Te = 120°K model were used. For the models containing $\frac{2}{3}$ helium, the gradients were taken directly from Trafton's model of the same effective temperature.

The corrected values of P, G_R, and x, calculated from equations 2.32, 2.30, and 2.33a respectively, have been used in all the models.

2.5 Adiabatic Gradient

The wet adiabatic gradient for the Jovian atmosphere was computed from Trafton's (1967) equation 18 through 21 using ammonia and water as saturable components. The equations used are given below.

$$\left.\frac{d\ln T}{d\ln P}\right|_{AD} \equiv G_A \approx \left[\frac{d\ln P_u}{d\ln T} + \frac{P_n}{P}\alpha + \frac{P_u}{P}\gamma\right]^{-1} \qquad (2.34)$$

$$\text{where } \frac{d\ln P_u}{d\ln T} \approx \frac{\bar{C}_{p,u}/R + P_n\alpha^2/P + P_u\gamma^2/P}{1 + P_n\alpha/P + P_u\gamma/P}, \tag{2.35}$$

$$P_n = A \exp(-\alpha), \text{ and } P_u = C \exp(-\gamma) \tag{2.36}$$

are the saturated vapor pressures of ammonia and water vapor respectively; ($P_n = 0$ if ammonia is unsaturated and similarly for water) and $\bar{C}_{p,u}$ is the specific heat at constant pressure for the uncondensable components.

The vapor pressure of ammonia was taken from the International Critical Tables (1928). The vapor pressure of water was taken from the Handbook of Chemistry and Physics (1954). The values of the constants in equations 2.36 are

$$\begin{aligned} \text{for} \quad & T<195^{\circ}K: \ \alpha = 3753.57/T, \ A = 9.940\times10^{9} \\ & T<273^{\circ}K: \ \gamma = 6194/T, \quad C = 3.236\times10^{10} \\ & T>273^{\circ}K: \ \gamma = 5273/T, \quad C = 1.148\times10^{9} \end{aligned} \tag{2.37}$$

The units of A and C are in mmHg.

The specific heat at constant pressure for a mixture is an average of the specific heats for each component weighted by its fractional abundance. Thus for an atmosphere composed of hydrogen and helium

$$\frac{\bar{C}_{p,u}}{R} = \alpha_1 \frac{C_{pH_2}}{R} + \alpha_2 \frac{C_{pHe}}{R} \quad . \tag{2.38}$$

$C_{pHe}/R = 2.500$ at all temperatures. C_{pH_2}/R is a function of temperature and, to a very slight degree, of pressure. Calculated values for the specific heat of hydrogen may be found in NBS Circular 546 (1955), and are also shown in Table 2.3. I have taken account of the variation in pressure by the empirical equation

$$\frac{C_{pH_2}}{R} = \frac{C_{pH_2}(0)}{R} \left(1+10^{-2}\left(\frac{P}{760}\right)e^{-\frac{T}{70}}\right) \tag{2.39}$$

where $C_{pH_2}(0)$ is the specific heat at zero pressure. In using this equation I have assumed that pressure due to helium has the same effect on the specific heat as pressure due to hydrogen.

Table 2.3

$\frac{C_p}{R}$ for H_2 at Zero Pressure

T(°K)	C_p/R	T(°K)	C_p/R	T(°K)	C_p/R
		190	3.244		
80	2.567	200	3.280	320	3.483
		210	3.312		
100	2.714	220	3.340	340	3.494
110	2.785	230	3.366		
120	2.857	240	3.387	360	3.501
130	2.927	250	3.407		
140	2.993	260	3.424	380	3.507
150	3.053	270	3.438		
160	3.108	280	3.450	400	3.510
170	3.158	290	3.460		
180	3.204	300	3.469		

2.6 Choice of Gradient

The atmosphere will be in radiative equilibrium, i.e. the actual atmospheric gradient will be the radiative gradient when the radiative gradient is less than the adiabatic gradient. When it is greater, the atmosphere will be in convective equilibrium, and the atmospheric gradient will be the adiabatic gradient.

3. The Microwave Absorption Coefficient

3.1 General

A total microwave absorption coefficient is the sum of the contributions to the absorption coefficient by the various constituents in the medium. For Jupiter the absorption coefficient is

$$\kappa = N_{H_2}\alpha_{H_2} + N_{He}\alpha_{He} + N_{NH_3}\alpha_{NH_3} + N_{CH_4}\alpha_{CH_4} + N_{H_2O}\alpha_{H_2O} \quad (3.1)$$

where κ is the total absorption coefficient (cm^{-1}),

α is the atomic absorption coefficient (cm^2), and

N is the abundance of each molecule considered (cm^{-3}).

The strength of the absorption coefficient, α, depends on the size of the molecular dipole moment. Hydrogen, helium and methane have no permanent dipole moment, but they have a small absorption coefficient due to a collision-induced dipole moment. In spite of their small atomic absorption coefficients, hydrogen and helium, because of their large abundances in the Jovian atmosphere, produce a small but significant absorption at millimeter wavelengths. Naumov and Khizhnyakov (1965) have estimated the absorption due to methane (mixing ratio $\lesssim .003$) in the Jovian atmosphere. They find that the absorption from methane is very much less than it is for hydrogen.

Both water and ammonia have large permanent dipole moments and thus both have large atomic absorption coefficients. Ammonia is, by far,

the strongest absorber of microwave radiation in the Jovian atmosphere. The largest contribution to the ammonia absorption comes from an inversion transition centered at a frequency of 0.78 cm^{-1}, which is pressure broadened to cause significant absorption throughout the microwave spectrum. There is also a small contribution at millimeter wavelengths from the low frequency tail of the pressure broadened rotational spectrum of ammonia which lies in the far infrared.

Although water has not been observed in the Jovian atmosphere, there is good likelihood of its existence at levels whose temperatures are in the neighborhood of 260°K and higher. The Jovian atmosphere at these levels is opaque to radiation which has a wavelength shorter than a few centimeters due to the strong ammonia absorption; thus water vapor could have a directly observable effect only at longer wavelengths. The microwave absorption coefficient of water and its evaluation for conditions in the Jovian atmosphere are calculated in Appendix B. The results of these calculations, as applied to Jupiter, are as follows. For the likely case that there are roughly equal quantities of ammonia and water vapor in the Jovian atmosphere at the level where the temperature is 270°K, water vapor absorption is less than 1% of the ammonia absorption at a wavelength of 2.5 cm. At longer wavelengths both absorption coefficients go roughly as ν^2 so I feel that absorption at all wavelengths due to water vapor is very much smaller than that due to ammonia.

Because of their negligible contributions, I have not included absorption by methane or water in the calculations of the total microwave absorption coefficient.

3.2 Ammonia

The inversion spectrum of ammonia has been extensively studied. Townes and Schawlow (1955) give a good review of the theory and the empirical results. A short description of the ammonia molecule, its energy levels, associated degeneracies, and other quantities which are needed for the computation of the absorption coefficient can be found in Appendix A. The final equations needed to compute the ammonia absorption coefficient are referenced on pages 109-110.

3.3 Hydrogen and Helium

The microwave absorption coefficient due to hydrogen and helium has been computed by extrapolating the values computed at somewhat higher frequencies by Trafton (1966a, 1966b, 1967) down to microwave frequencies. The absorption coefficient is the sum of a purely translational component and a rotational-translational component, which lies on the high frequency wing of the translational component. The microwave region of the spectrum lies at the low frequency end of both of these components.

Trafton gives the absorption coefficient due to hydrogen with enhancement from helium as

$$\alpha_{H_2} = \frac{1}{c} (N_{H_2} A_\nu + N_{He} B_\nu) \qquad (3.2)$$

where A_ν and B_ν are his "absorption coefficients."

At low frequencies, below about 20 cm^{-1}, the absorption coefficient is proportional to ν^2 so we may write

$$\left.\begin{matrix} A_\nu \\ B_\nu \end{matrix}\right\} = \nu^2 \times \left\{\begin{matrix} A_1 \\ B_1 \end{matrix}\right. \qquad (3.3)$$

where A_1 and B_1 are the values of A_ν and B_ν respectively at a frequency of 1 cm^{-1}.

One must now find A_1 and B_1 as functions of temperature. Trafton (1966a) has given me tabulated values of A_ν and $A_\nu+B_\nu$ for temperatures between 95°K and 250°K, and for frequencies down to 32 cm^{-1}. This is not quite low enough for the ν^2 law to apply.

To find A_1 and B_1, Trafton's values of A_ν and $A_\nu+B_\nu$ were plotted against frequency on log-log paper for selected temperatures between 95° and 250°K. In these coordinates an absorption coefficient proportional to ν^2 shows up as a straight line with slope two. Therefore curves were fit through all the points representing a given temperature, and they were extended smoothly to lower frequencies with slopes that asymptotically approached two. These curves for A_ν are shown in Figure 3.1. The fitting was judged to be fairly accurate (~10%) as Trafton's lowest frequencies come close to the region in which the ν^2-law applies.

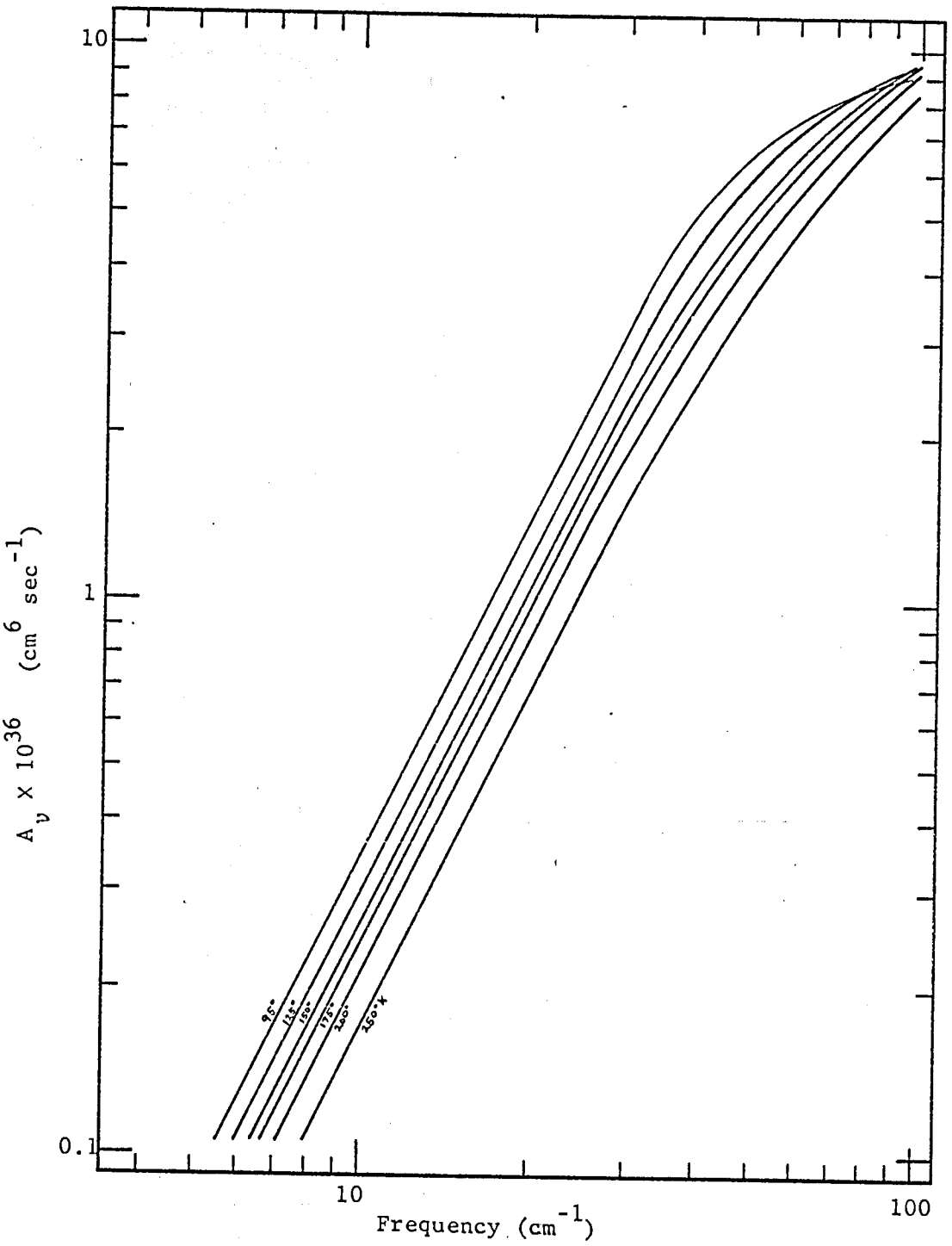

Figure 3.1

The Low Frequency Tail of A_ν

From these graphs the values of A_ν and B_ν at a frequency of 1 cm^{-1} could be read off. These values were then plotted versus temperature on log-log paper as shown in Figure 3.2. Straight lines were fitted through both sets of points with a preference towards fitting the region near 150°K most accurately as that is the observed radiometric temperature of Jupiter at millimeter wavelengths, where the hydrogen-helium contribution is the strongest.

A straight line of slope -0.8 fit the curve for A_1 very well from 95 to 250°K, and a line of slope -0.61 fit the data for B_1 to within 7%.

The results are

$$A_1 = 0.377 \times 10^{-38} \left(\frac{T}{100}\right)^{-0.8}$$

and (3.4)

$$B_1 = 0.535 \times 10^{-38} \left(\frac{T}{100}\right)^{-0.61} .$$

Thus

$$\alpha_{H_2} = \frac{1}{c} \times 10^{-38} \left[0.377\ N_{H_2} \left(\frac{T}{100}\right)^{-0.8} + 0.535\ N_{He} \left(\frac{T}{100}\right)^{-0.61}\right] \nu^2 . \quad (3.5)$$

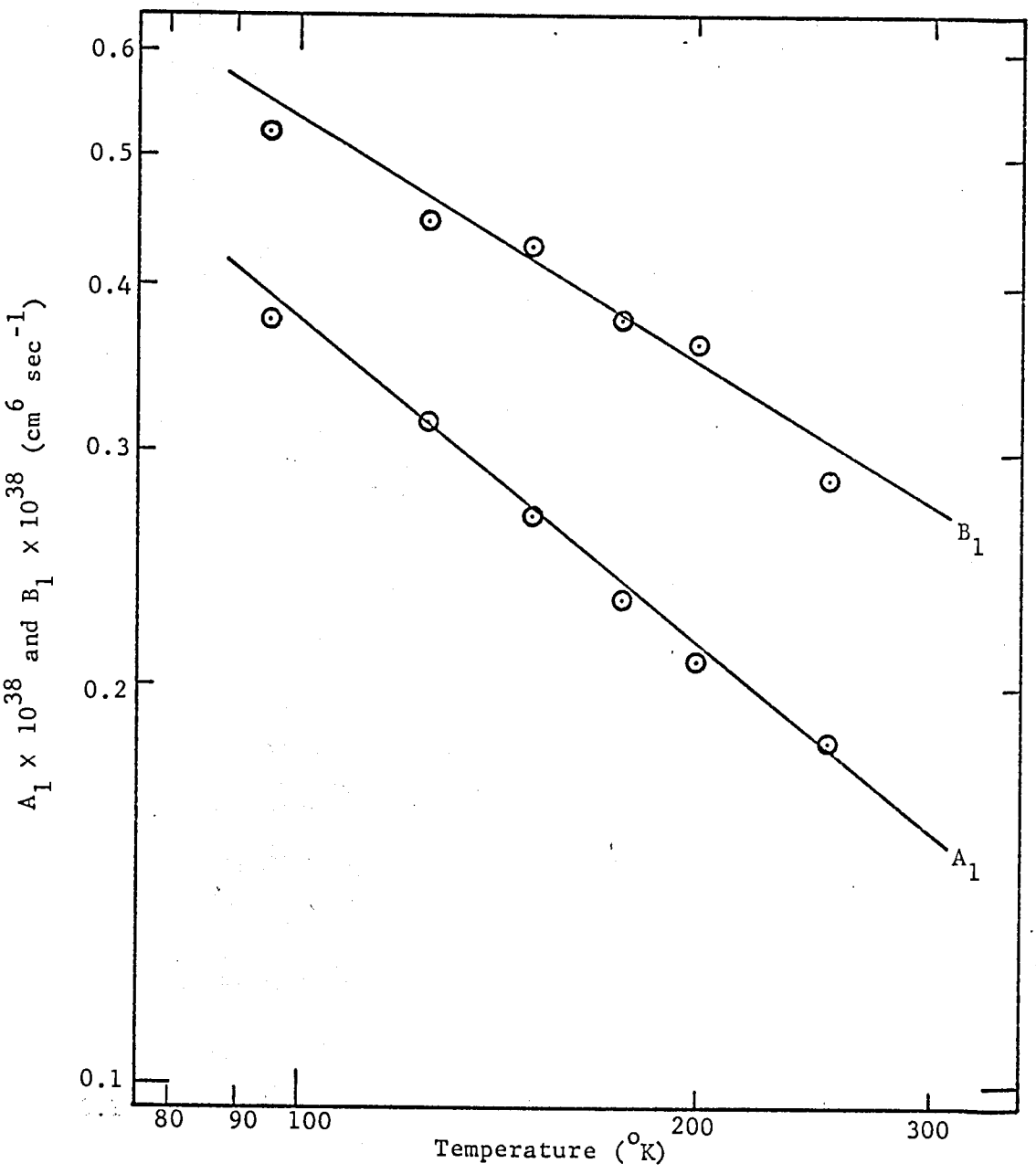

Figure 3.2

Hydrogen and Helium Absorption Coefficients
Constants - A_1 and B_1

4. Radio Brightness Temperature

4.1 Temperature Distribution

Thus far in the discussion no mention has been made of any variation of the effective temperature of the planet with longitude or latitude. Trafton (1967) has shown that the rotation of Jupiter is rapid enough so that no significant variation of temperature with longitude is to be expected.* However a variation with latitude is expected and must be considered.

Since Jupiter's rotational axis is tilted only 3^{o} to its orbital axis, the sun can be considered to be overhead at the Jovian equator. Thus the average rate at which energy is absorbed per unit area due to insolation, E_{ins}, is given by

$$E_{ins} = \frac{S}{a^2}(1-A)\frac{\cos\phi}{\pi} \equiv 4\sigma T_{ins}^{4}\frac{\cos\phi}{\pi} \qquad (4.1)$$

where S is the solar constant,

a is the semimajor axis in A. U.,

A is the Bond albedo,

ϕ is the latitude, and

σ is the Stefan-Boltzmann constant.

T_{ins} is the effective temperature Jupiter would have if it radiated isotropically the same total amount of energy that it received

---

*The temperature drop from the evening limb to the morning limb is about $\frac{1}{2}^{o}$K.

from the sun. Taylor (1965), Walker (1966) and others have shown T_{ins} to be about $104 \pm 3^{\circ}K$.

Additional energy may be delivered uniformly to the surface from an internal source at the rate E_{int} per unit area. This can be written in terms of an effective internal temperature, T_{int}:

$$E_{int} = \sigma T_{int}^{4} . \qquad (4.2)$$

Thus the total rate at which energy is absorbed at the Jovian "surface" is

$$E_{abs} = E_{ins} + E_{int} = \sigma[\tfrac{4}{\pi} T_{ins}^{4} \cos\phi + T_{int}^{4}] . \qquad (4.3)$$

Since more energy is absorbed at lower latitudes than at higher, a thermal gradient exists which drives energy from the equatorial regions towards the polar regions, and this, in turn, tends to equalize the temperature over the entire surface. The existence of such a tangential flow of heat is in direct contradiction to the assumption made in Chapter 2 that the heat flow was purely radial. However I believe that this tangential flow must be so small compared with the radial flow that the models are still valid. I have not seen any calculations dealing with the transfer of heat from one latitude to another on Jupiter, so I will just offer a few qualitative arguments against a strong tangential heat flow. Since the tangential temperature gradient on Jupiter must be extremely small compared with the radial temperature gradient--about $\frac{1}{3000}$ as great if the difference in temperature between the equator and the

poles is about $60^{o}K$, conductive and radiative transfer of heat in the tangential direction is negligible. The only way a large amount of heat could be transferred towards the poles would be by winds. However Jupiter's large size and high rotation rate combine to give a very strong Coriolis interaction which deflects all winds to an east-west direction. In support of this, observations of markings on Jupiter show only an east-west motion. A more detailed analysis is left to the future.

The two possible extreme cases for the temperature distribution are:

1. The energy is reradiated from the same latitude in which it was absorbed. The effective temperature T_e is then given by

$$T_e^4 = \frac{4}{\pi} T_{ins}^4 \cos\phi + T_{int}^4 . \qquad (4.4)$$

2. The absorbed energy is uniformly distributed over the entire surface of the planet before it is reradiated. In this case the effective temperature T_{eo} is given by

$$T_{eo}^4 = T_{ins}^4 + T_{int}^4 . \qquad (4.5)$$

The contribution to the radio temperature from a band of latitude is approximately proportional to its projected area against the plane of the sky. This band and the associated nomenclature are illustrated in Figure 4.1. In order to evaluate the strength of the effect

that the variation of effective temperature with latitude may have on the radio temperature, both T_e and T_{eo} have been plotted against s, the fraction of projected area lying between latitudes $\pm \phi$. This plot is shown in Figure 4.2.

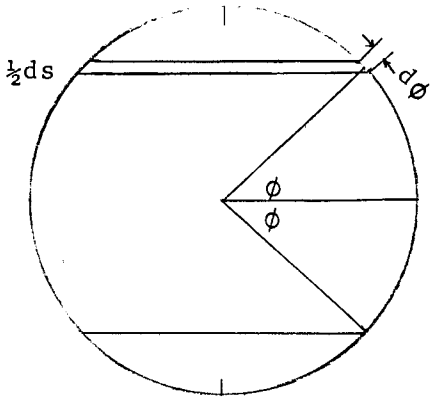

Figure 4.1
Schematic of Projected Area

s is the fraction of projected area which lies between latitudes $\pm \phi$.

$$s = \frac{2}{\pi}\phi + \frac{\sin 2\phi}{\pi} \qquad (4.6)$$

Figure 4.2

Effective Temperature of the Jovian Surface for Various Amounts of Internal Heating

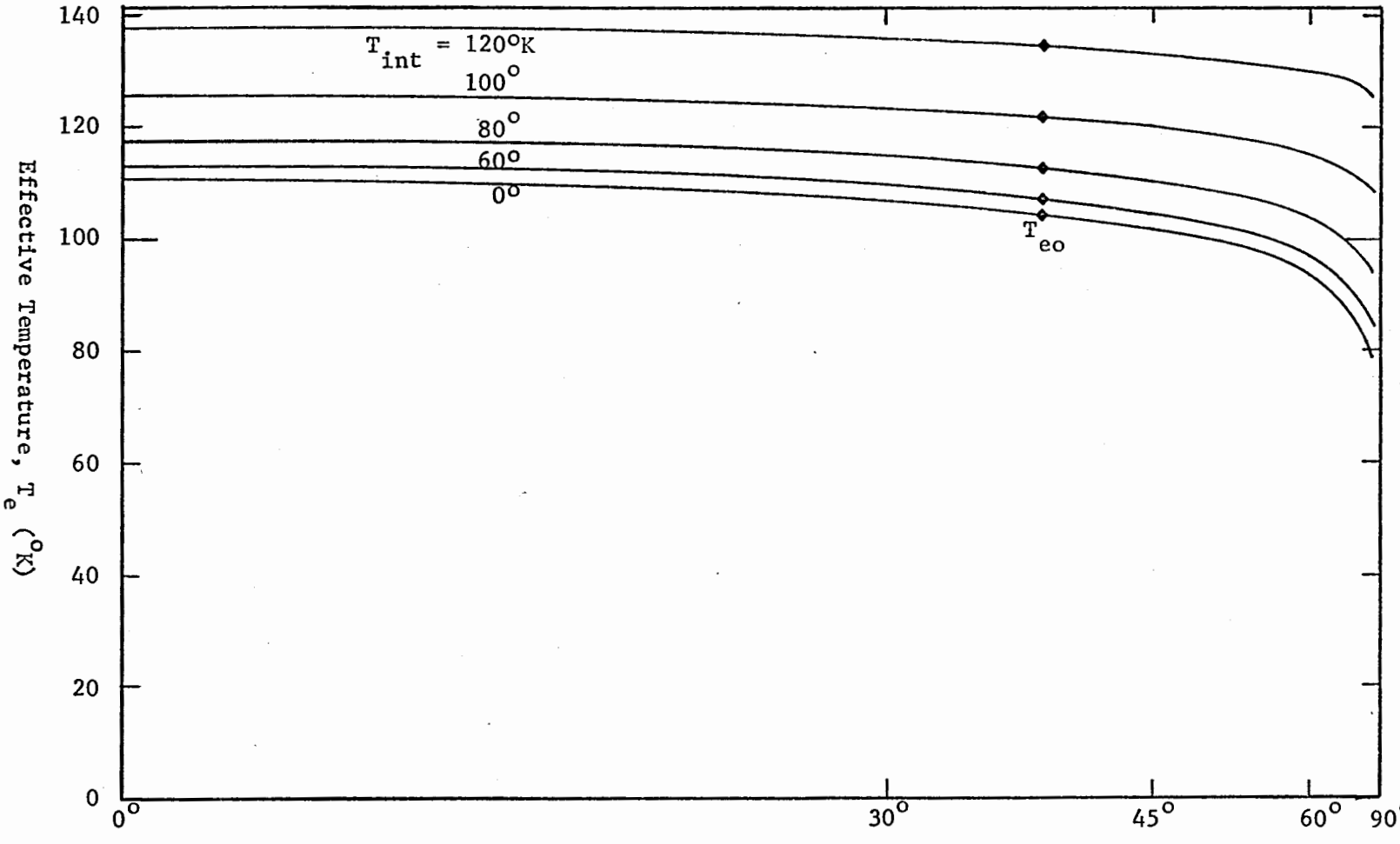

According to Trafton (1967), Low and Davidson (1968), and in the conclusions of this thesis, an effective temperature near 130^{o} appears to be reasonable for Jupiter. Referring to Figure 4.2, one can see that such a high effective temperature requires a strong internal heat source, and in this case, even if there is no transfer of energy from one latitude to another, the effective temperature remains quite uniform over 90% of the projected area. Because of this, I have made the simplifying assumption in the calculation of the radio temperature, that an atmospheric model with a single effective temperature can be used, and thus, as far as the structure of the atmosphere is concerned, Jupiter is spherically symmetric.

4.2 Equations Used to Predict the Brightness Temperature

The flux per unit frequency interval, $\mathcal{F}_\nu$, emitted by an atmosphere in thermal equilibrium can be related to the temperature as a function of optical depth, τ_ν, through a convenient formula (Aller (1963)):

$$\mathcal{F}_\nu = 2\pi \int_o^\infty B_\nu (T[\tau_\nu]) \; E_2(\tau_\nu) d\tau_\nu \qquad (4.7)$$

where $E_n(x)$ is the n^{th} exponential integral function and is defined by

$$E_n(x) = \int_1^\infty \frac{1}{y^n} e^{-xy} dy,$$

and $B_\nu(T)$ is the Planck function per unit frequency interval.

When $\frac{hc\nu}{kT} \ll 1$, as is the case for microwaves and Jovian temperatures, the Rayleigh-Jeans approximation to the Planck function can be used:

$$B_\nu(T) \approx \frac{2kT}{\lambda^2} \quad . \tag{4.8}$$

Radio astronomers measure the flux density at a given frequency in terms of the brightness temperature, T_b, which is the temperature of a black body which emits flux density, $\mathcal{F}_\nu$, at that frequency. With the Rayleigh-Jeans approximation the relationship between the flux density and the brightness temperature is simply

$$\mathcal{F}_\nu = \pi B_\nu = \frac{2\pi k T_b}{\lambda^2} \quad . \tag{4.9}$$

With the use of equations 4.7 through 4.9, an equation for the brightness temperature can be written:

$$T_b(\nu) = 2\int_o^\infty T(\tau_\nu) E_2(\tau_\nu) d\tau_\nu = -2\int_{\tau=0}^\infty T(\tau_\nu) dE_3(\tau_\nu) \tag{4.10}$$

The optical depth is given as a function of frequency and physical depth, x (measured inwards) by the equation

$$\tau_\nu(x) \equiv \int_{-\infty}^x \kappa_\nu(x')dx' = \sum_i \int_{-\infty}^x \alpha_{\nu i} L_o \rho_i dx' = \sum_i \int_o^{q_i(x)} \alpha_i L_o dq_i' \tag{4.11}$$

where κ_ν is the microwave absorption coefficient (cm^{-1}),

$\alpha_{\nu i}$ is the atomic absorption coefficient for molecules of type i (cm^2),

ρ_i is the density of molecules of type i (amagats), and

q_i is the total quantity of gas of type i which lies above x (cm-amagats).

The atomic absorption coefficients for ammonia and hydrogen were calculated by using the equations given in Chapter 3. For ammonia all transitions were considered which originated from levels with $J \leq 17$. However a careful analysis revealed that about $\frac{1}{3}$ of these lines were so weak that removing them had no significant effect* other than a consequent reduction in running time on the computer. The lines which were removed are listed in Table 4.1 on the next page by the J and K values of the lower levels. (Remember J and K don't change for inversion transitions.) These lines were judged to contribute less than the $\frac{1}{1000}$ to the total absorption coefficient at all frequencies between .05 and $10 cm^{-1}$, and at temperatures less than $300^{\circ}K$ and pressures of a few atmospheres. Most of these lines contributed less than 10^{-5} to the total absorption coefficient.

The quantities of the various gases lying above any given level are needed not only for the computation of optical depth but also in

---

*Removing these lines increased the computed brightness temperature by less than $.01^{\circ}K$ at all frequencies.

order to make a more thorough comparison between Jupiter with its observed molecular abundances and the models.

J	K	J	K
10	1-2	14	1-8
11	1-2	15	1-11,13
12	1-4	16	1-14
13	1-5	17	A11

Table 4.1

Lines Not Included in the Computation of the NH_3 Absorption Coefficient

Since the fractional concentrations of hydrogen, helium, and methane are constant throughout the atmosphere, the quantities of these gases can be calculated from the condition of hydrostatic equilibrium:

$$P = g\int_{-\infty}^{x} \rho dx = g\int_{o}^{M} dm = gM \qquad (4.12)$$

where M is the mass per unit area of atmosphere which lies above the level where the pressure is P.

Hydrogen and helium are the only major constituents so

$$M = \frac{L_o}{N_o}(2q_{H_2} + 4q_{He}) = \frac{L_o}{N_o} q_{H_2}\left(2+4\frac{\alpha_2}{\alpha_1}\right) . \qquad (4.13)$$

From equations 4.12 and 4.13 one obtains

$$q_{H_2} = \frac{N_o}{L_o} \frac{\alpha_1}{2\alpha_1 + 4\alpha_2} \frac{P}{g} = 148.46 \frac{P}{g} \frac{\alpha_1}{\alpha_1 + 2\alpha_2} \qquad (4.14)$$

where the numerical constant is for q_{H_2} in km-amagats, P in mmHg and g in cgs units.

The amounts of helium and methane lying above this same level are simply given by

$$q_{He} = \frac{\alpha_2}{\alpha_1} q_{H_2} \text{ and } q_{CH_4} = \frac{\alpha_5}{\alpha_1} q_{H_2} . \qquad (4.15)$$

Since the concentration of ammonia is not dependent simply on its mixing ratio, but also on its vapor pressure (see pg. 44) the quantity of ammonia lying above a given level must be found by direct integration:

$$q_{NH_3} = \int_{-\infty}^{x} \left(\frac{P_{NH_3}}{760}\right) \left(\frac{273}{T}\right) dx' . \qquad (4.16)$$

Equation 4.16 was numerically integrated using the trapezoidal rule and the step-sizes were, at first, taken to be the differences in the tabulated atmospheric levels which are given by Trafton and which are used also in the present models. However since the quantity of ammonia increased by a factor of almost 3 between some of the levels, it was thought that this integration step-size was too large to give sufficiently accurate

results. Therefore intermediate levels, halfway between the adjoining levels, were mathematically constructed. At these intermediate levels the temperature and pressure of ammonia were computed and equation 4.16 integrated with ½ the original step-size.

The intermediate levels were constructed from an interpolation procedure involving the equation of hydrostatic equilibrium

$$\frac{dP}{dT}\frac{dT}{dx} = g\rho = \frac{\mu g}{R}\frac{P}{T} \quad . \tag{4.17}$$

In the region of the atmosphere where the concentration of ammonia is high, the temperature is very close to a linear function of depth. Therefore in the region between two adjoining levels, designated by subscripts n and n+1,

$$\frac{dT}{dx} \approx \frac{T_{n+1} - T_n}{x_{n+1} - x_n} \quad . \tag{4.18}$$

With $\frac{dT}{dx}$ given by equation 4.18 the solution to equation 4.17 is

$$\frac{P}{P_n} = \frac{T}{T_n}^{\frac{\mu g}{R}\left(\frac{x_{n+1} - x_n}{T_{n+1} - T_n}\right)} \quad . \tag{4.19}$$

At the intermediate levels $x = \frac{1}{2}(x_n + x_{n+1})$, $T = \frac{1}{2}(T_n + T_{n+1})$, and the corresponding value for P is given by equation 4.19. The pressure of ammonia is calculated in the same way as it is for any of the tabulated levels.

The result of this more complicated integration procedure is a reduction in the calculated amount of ammonia lying above any given level by about 4% and an increase in the calculated brightness temperature of about $0.2^{o}K$. The remaining error due to the step-wise integration of equation 4.16 has been estimated to be about $\frac{1}{3}$ the size of the correction which has just been found, and is inconsequential.

For the calculation of the brightness temperature, the second form of equation 4.10 is more suitable for numerical integration than the first form. This is because the value of E_2 changes by a large and varying amount between the integration steps. The temperature, on the other hand, changes by generally less than 5% between adjacent steps. For numerical integration equation 4.10 takes the form

$$T_b(\nu) = 2 \sum_{n=0}^{\infty} \langle T \rangle_n^{n+1} \left[E_3(\tau_n[\nu]) - E_3(\tau_{n+1}[\nu]) \right] \qquad (4.20)$$

where the subscript n again signifies the n^{th} atmospheric level with

$\tau_0 \equiv 0$ and,

$$\langle T \rangle_n^{n+1} \equiv \int_{E_3(\tau_{n+1})}^{E_3(\tau_n)} T(\tau) dE_3(\tau) / \left[E_3(\tau_n) - E_3(\tau_{n+1}) \right] \qquad (4.21)$$

The summation in equation 4.20 was considered to be complete when τ exceeded 3.5. This was accomplished by setting E_3 to zero for the first level in which τ exceeded 3.5. The error in the calculated brightness temperature which results from this is always less than $0.2^{o}K$.

As can be seen from equation 4.21, $\langle T \rangle_n^{n+1}$ is an average value of the temperature in the region between the n^{th} and $n+1^{th}$ levels. Equation 4.21 cannot be properly evaluated as T is known at only the end points of the interval over which the integration is performed. Therefore I have used the approximation

$$\langle T \rangle_n^{n+1} \approx \frac{1}{2}[T(\tau_n) + T(\tau_{n+1})] \quad . \tag{4.22}$$

In order to estimate the accuracy of this approximation, a plot of the known paired values of $T(\tau)$ and $E_3(\tau)$ for one model atmosphere was made at one frequency, and a smooth curve was drawn connecting these points. The integral in equation 4.10 was then determined with a planimeter. The brightness temperature calculated from this procedure was about $0.6^{o}K$ lower than that calculated from equation 4.20. The total error in the calculations is probably less than the $1^{o}K$.

The dependence of the brightness temperature on the absorption by the rotational lines of ammonia and on the absorption by hydrogen was also determined. At a frequency of $0.1 cm^{-1}$ the rotational lines decrease the brightness temperature about $0.12^{o}K$ and hydrogen causes an additional decrease of about $0.58^{o}K$. As was to be expected these effects are inversely proportional to the square of the frequency.

The results of the radio temperature calculations for various Jovian model atmospheres are shown in Figures 4.3 to 4.6. Each spectrum plot is labeled by a model number. The defining parameters for each model are given in Table 5.1.

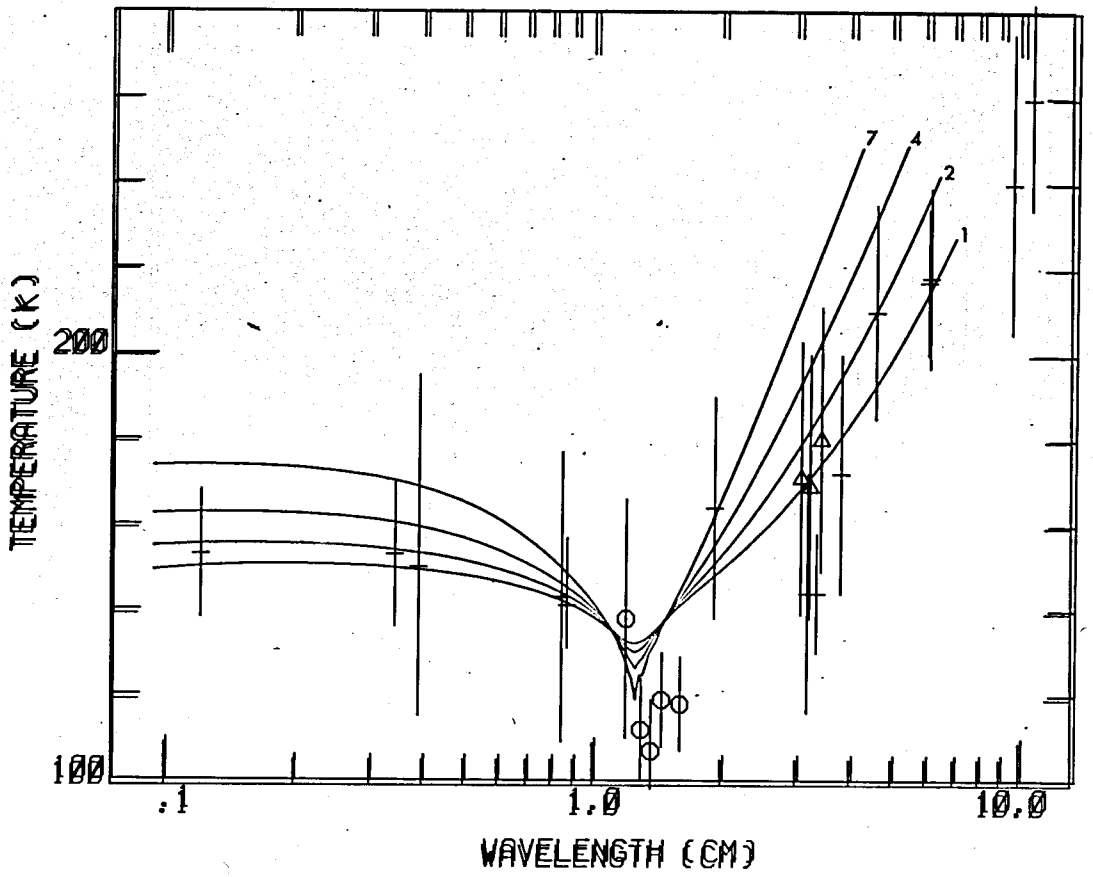

Figure 4.3

Calculated Brightness Temperature of Jupiter

Dependence on Effective Temperature

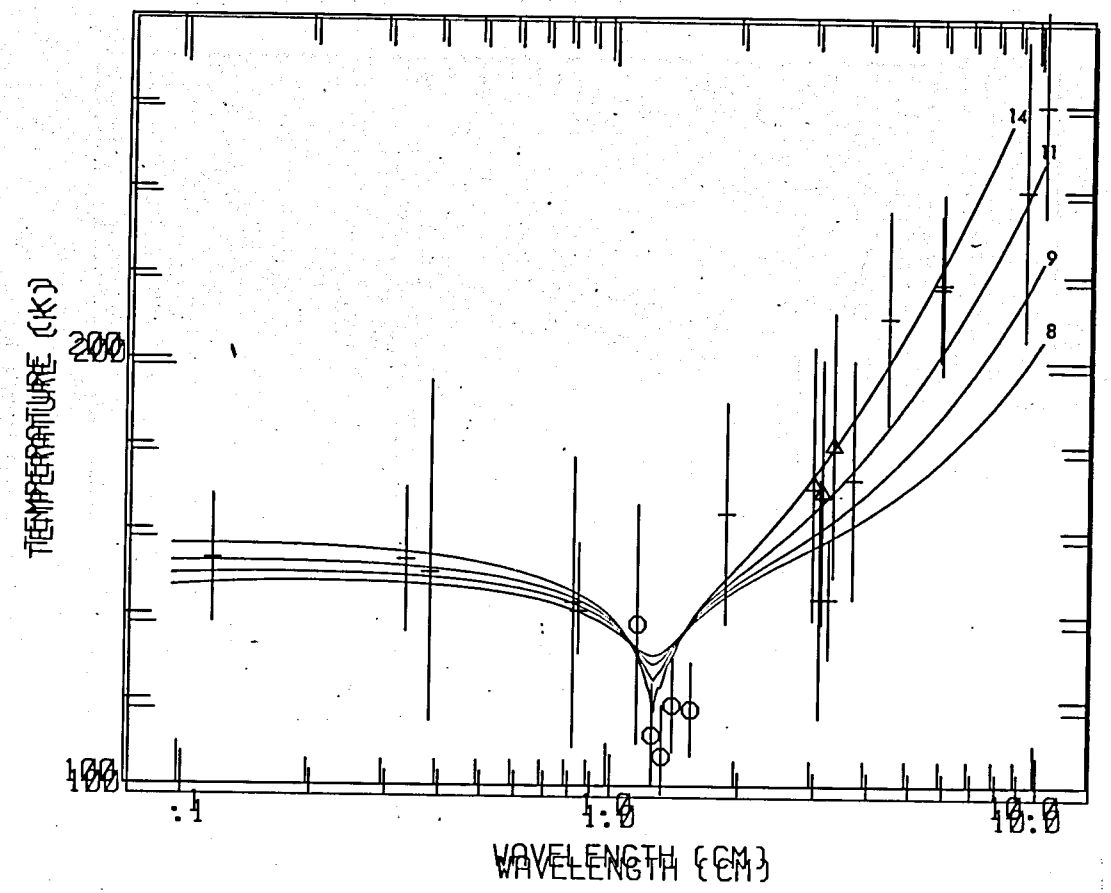

Figure 4.4

Calculated Brightness Temperature of Jupiter

Dependence on Effective Temperature

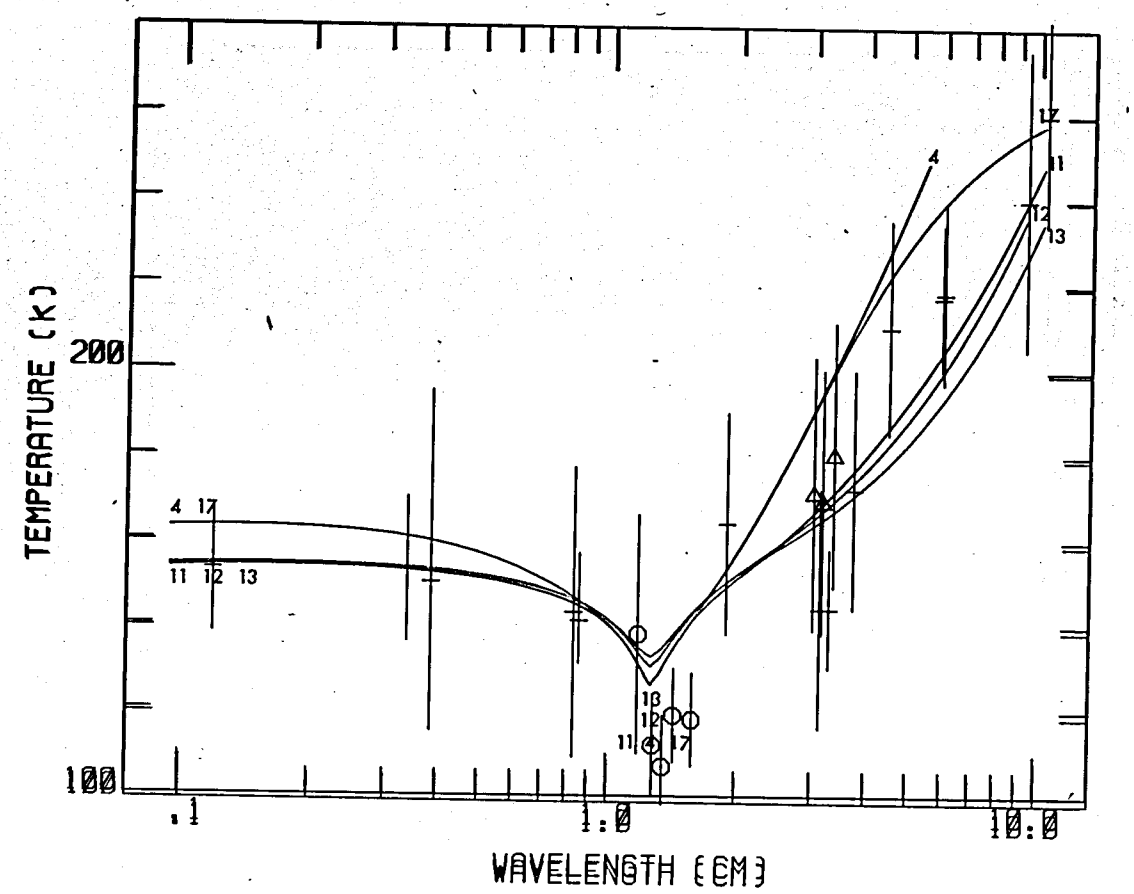

Figure 4.5

Calculated Brightness Temperature of Jupiter

Upper Curves Show Effect of Ground at 270°K.

Lower Curves Show Dependence on the Mixing Ratio of Helium.

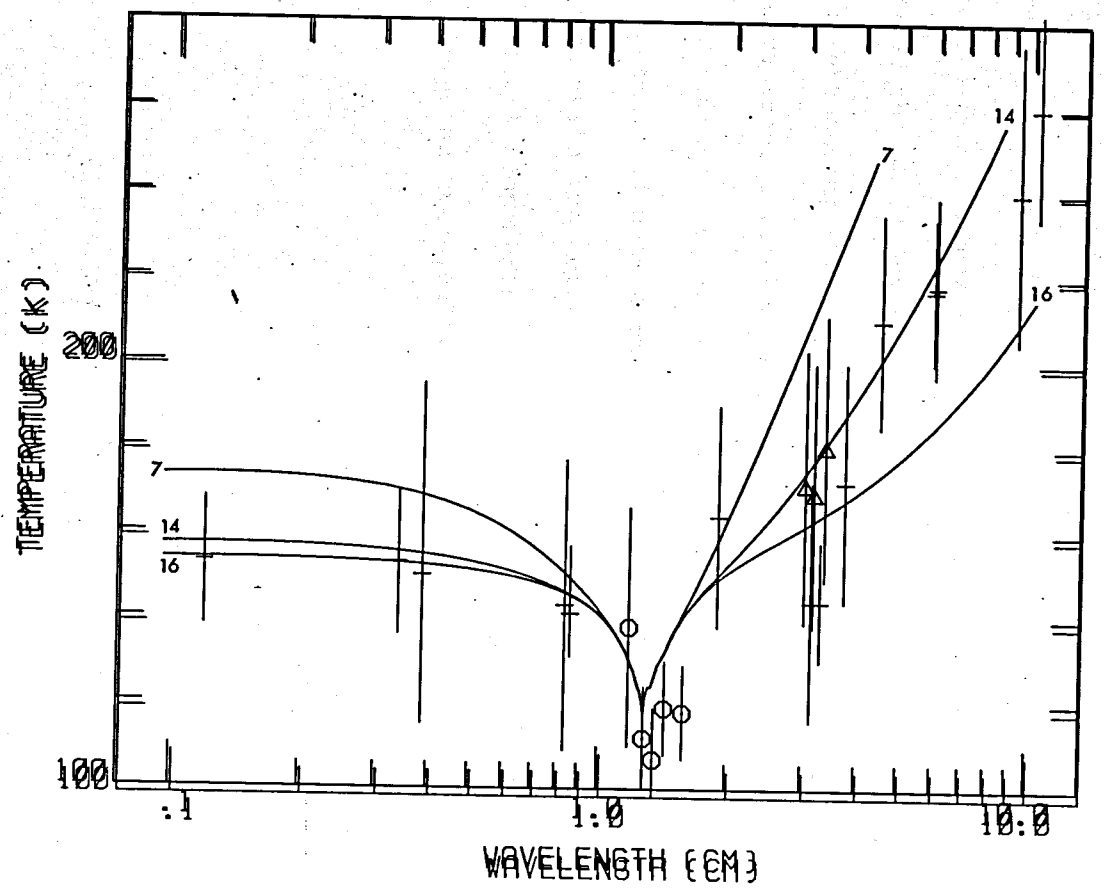

Figure 4.6

Calculated Brightness Temperature of Jupiter

Dependence on the Mixing Ratio of Ammonia

4.3 Observed Radio Spectrum

A comparison between the theoretically calculated thermal component of the microwave spectrum and the observed spectrum must take account of the existence of a non-thermal component in the microwave radiation. This non-thermal component is very weak at 1 cm. wavelength but is dominant at 10 cm. Dickel, Degioanni, and Goodman in a forthcoming paper have gathered together the reliable microwave observations, corrected them for revised estimates of the flux densities of the sources used for calibration, and have attempted to separate the thermal and non-thermal components. The pertinent observations together with the corrected temperatures, and preliminary values for the thermal components are given in Table 4.2. The thermal spectrum is also shown graphically in Figure 4.7 and in the plastic overlay.

Table 4.2

Observed Brightness Temperature

Source	Wavelength (cm)	Published Temp. (^{o}K)	Corrected Temp. (^{o}K)	Thermal Temp. (^{o}K)
Low (1965)	0.12	153±15	153±15	153±15
Epstein (1968)	0.34	140±16	153±17	153±17
Kislyakov and Lebskii (1968)	0.387	150^{+45}_{-35}	150^{+45}_{-35}	150^{+45}_{-35}
Thornton and Welch (1963)	0.835	144±34	144±34	143±34
Law and Staelin (1968)	1.18	141±28	141±28	138±28
Law and Staelin (1968)	1.28	116±12	116±12	112±12
Law and Staelin (1968)	1.35	111±12	111±12	107±12
Law and Staelin (1968)	1.43	124±11	124±11	119±11
Law and Staelin (1968)	1.58	124±11	124±11	119±11
Dickel (1967a)	1.9	174±25	174±25	164±26
Giordmaine, Alsop, Townes and Mayer (1959)	3.03	171±20	200±35	171±32
Mayer, McCullough and Sloanaker (1958)	3.15	145±26	170±31	144±28
Giordmaine et al (1959)	3.17	173±30	202±35	169±31
Bibinova, Kuzmin and Salomonovich (1962)	3.3	193	175±12	144±14
Giordmaine et al (1959)	3.36	189±30	221±35	180±31
Dickel (1964)	3.75	226±34	220±33	172±28
Dickel (1967a)	4.5	293±29	293±29	210±25
Dickel (1967b)	6.0	369±20	369±20	218±21
Morris, Whiteoak, and Tonking (1968)	6.0	366±7	366±7	217±17
Rose, Bologna, and Sloanaker (1963)	9.4	658±58	670±60	240±35
Berge (1966)	10.4	260	260±26	260±26
Kalaghan and Wulfsberg (1968)	0.86	142^{+16}_{-10}	142^{+16}_{-10}	141^{+16}_{-10}

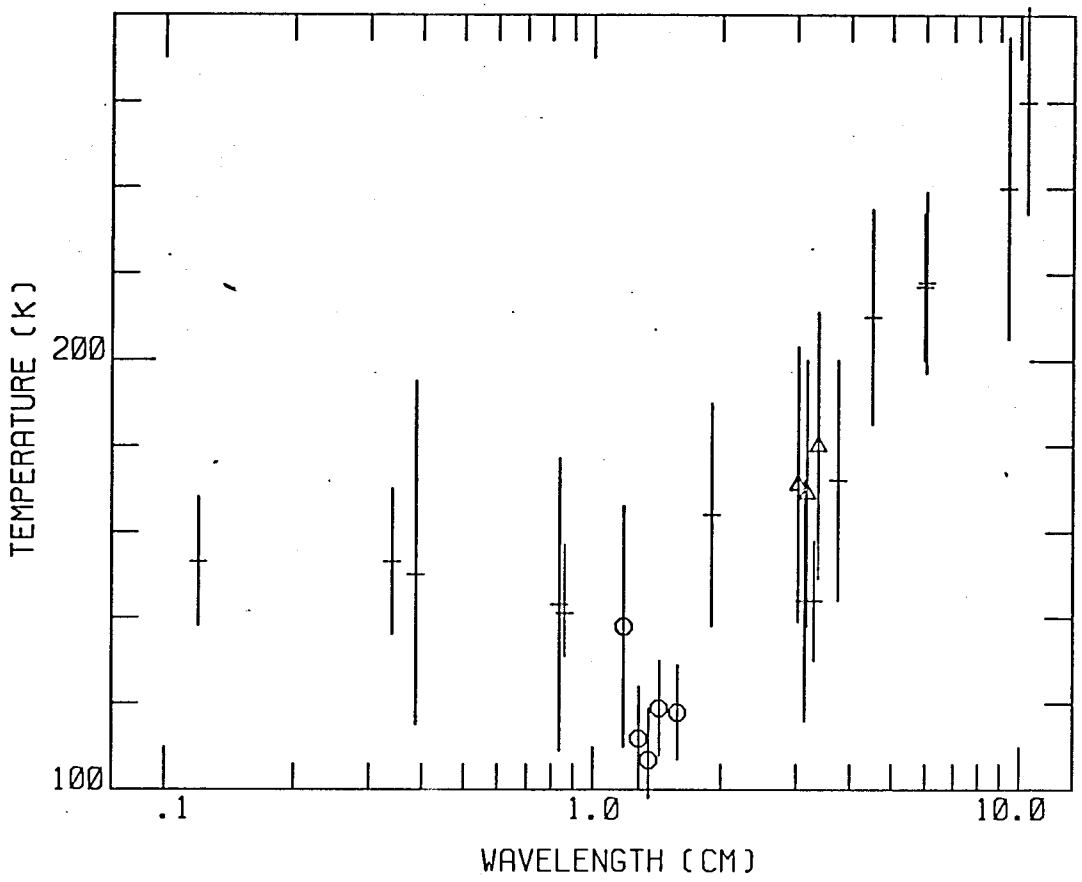

Figure 4.7

Observed Brightness Temperature of Jupiter

Observations marked by circles and triangles were published in the same paper.

5. Conclusion

5.1 The Properties of the Models

Table 5.1 contains a list of the models which were constructed along with their pertinent parameters. T_o is the boundary or stratospheric temperature, and T_c and P_c are the temperature and pressure at the top of the convective zone. The run of temperature, pressure, and depth for the various models are presented graphically in Figures 5.1 and 5.2. Although these graphs have been drawn for models having a mixing ratio for ammonia of .0008, they are valid for the models having an ammonia mixing ratio of .0002 also as the differences between these models are too small to be plotted on these graphs. This is because the portion of the atmosphere where the gradients differ between the two models, namely the region where, due to saturation, the local mixing ratio of ammonia is between .0002 and .0008 is only a few kilometers thick, and even there the differences in the gradients are less than 9%. However, these graphs should not be applied to models having an ammonia mixing ratio lying much outside these limits. If the mixing ratio were made much larger the wet adiabatic gradient would be significantly reduced. If the mixing ratio were made much smaller, the abundance of ammonia in the radiative region of the atmosphere would be reduced as would the radiative gradient. This is most pronounced with models having a high effective temperature.

The effect of the addition of water to the models is illustrated by model 15. As can be readily seen from Figures 5.1 and 5.2, the effect is negligible for temperatures below $250^{o}K$.

Table 5.1

List of Models Which Were Constructed and Their Characteristics

($\alpha_4 = 0$, $\alpha_5 = .003$ unless noted)

Model	Te(^{o}K)	$\frac{\alpha_2}{\alpha_1}$	α_3	Remarks	T_o(^{o}K)	T_c(^{o}K)	P_c(mmHg)
1	110	0	.0002		85.3	126.8	511
2	120	0	"		93.6	132.2	422
3	120	1	"		95.5	134.2	800
4	130	0	"		101.6	137.5	348
5	130	1	"		102.5	139.6	706
6	130	2	"		101.6	139.6	976
7	140	0	"		109.6	143.1	285
8	110	0	.0008		85.3	126.8	511
9	120	0	"		93.6	132.2	422
10	120	1	"		95.5	134.2	800
11	130	0	"		101.6	137.5	348
12	130	1	"		102.5	139.6	706
13	130	2	"		101.6	139.6	976
14	140	0	"		109.6	143.1	285
15	130	1	.0008	$\alpha_4 = .005$	102.5	139.6	706
16	140	0	.0032		109.6	143.1	285
17	130	0	.0002	"Ground" at 270^{o}K	101.6	137.5	348
18	130	1	.0002	"Ground" at 277^{o}K	102.5	139.6	706

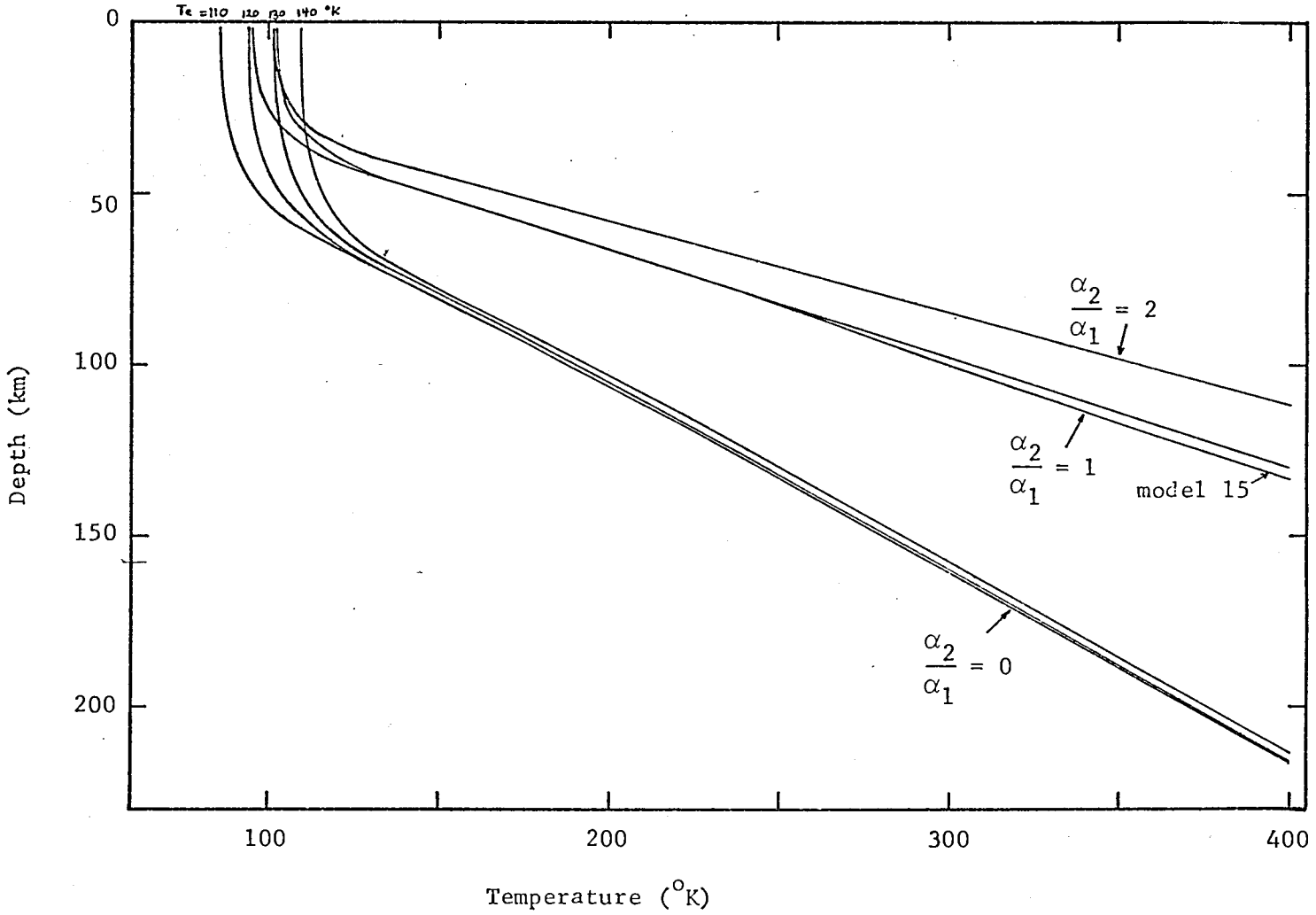

Figure 5.1

Depth versus Temperature for Jovian Model Atmospheres

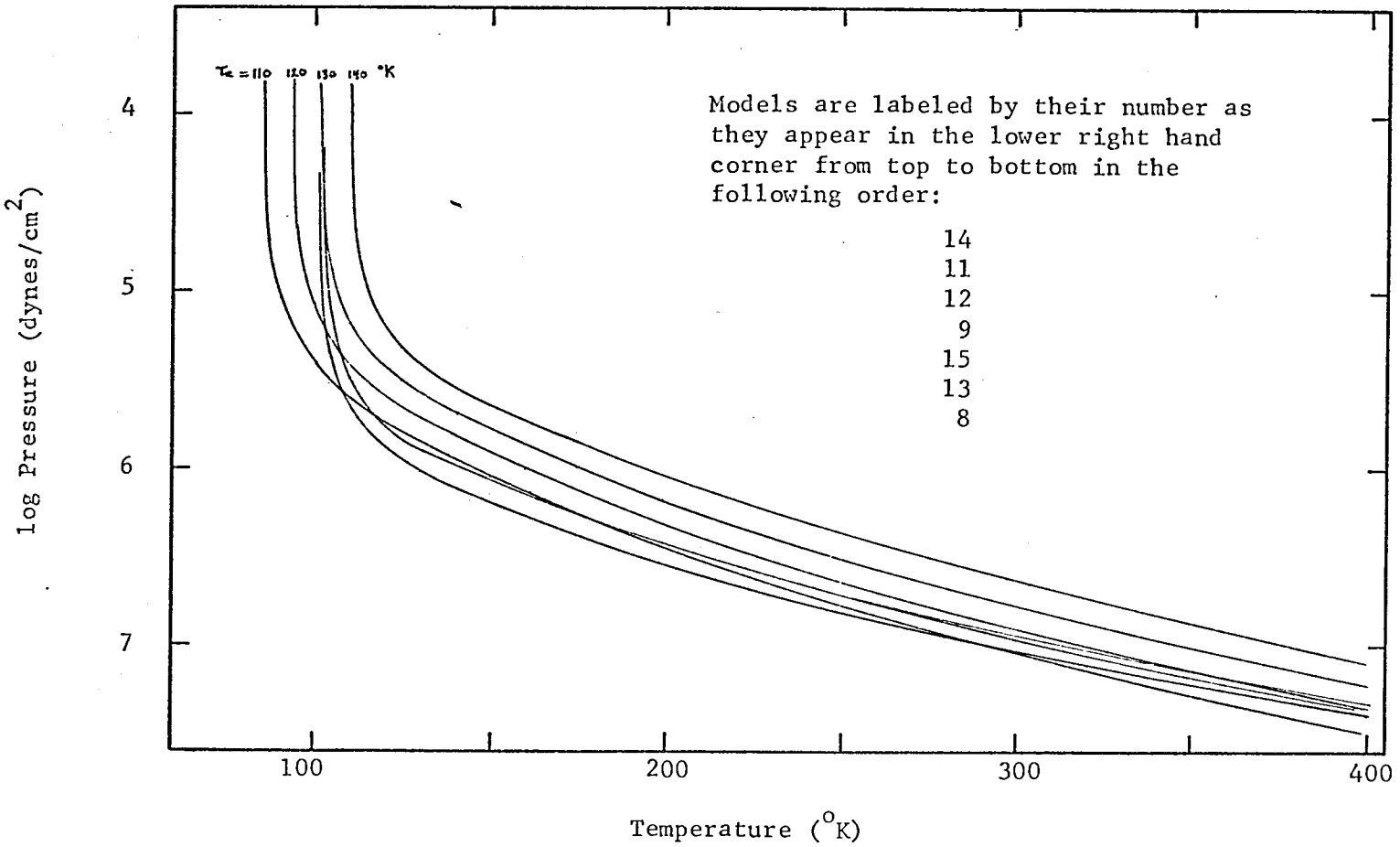

Figure 5.2

Pressure versus Temperature for Jovian Model Atmospheres

A comparison between these models and Trafton's models is given in Figures 5.3a and 5.3b. In each case only the region of the atmosphere which is in radiative equilibrium is shown. His models may be considered to be the limiting case for which the mixing ratio of ammonia is zero. As can be clearly seen, the major difference between the two models is the temperature at the top of the convection zone. This difference increases with effective temperature.

5.2 Comparison of the Models with the Observations

a) Microwave Comparisons

An overall comparison between the observations and the predicted microwave brightness temperatures shows that there is good basic agreement. However, the observations are not precise enough to conclusively select one or even a few models over the others although a few models can be definitely excluded.

For the purpose of the comparison, the spectrum can be divided into three regions, each of which behaves differently as the defining parameters for the models are varied. They are: i) short wavelength, <1.1 cm; ii) inversion region, 1.1-1.6 cm; and iii) long wavelength, >1.6 cm.

i) Short wavelength

This region is rather insensitive to variations in the model parameters. There is a slight dependence on effective temperature and ammonia mixing ratio which increases for very low mixing ratios. The ratio of helium to hydrogen has no effect on this portion of the spectrum. A comparison with the observations shows that a relationship exists between the lowest acceptable mixing ratio for ammonia and the effective temperature: for models with Te=130^{o}K the lower limit for α_3 is about

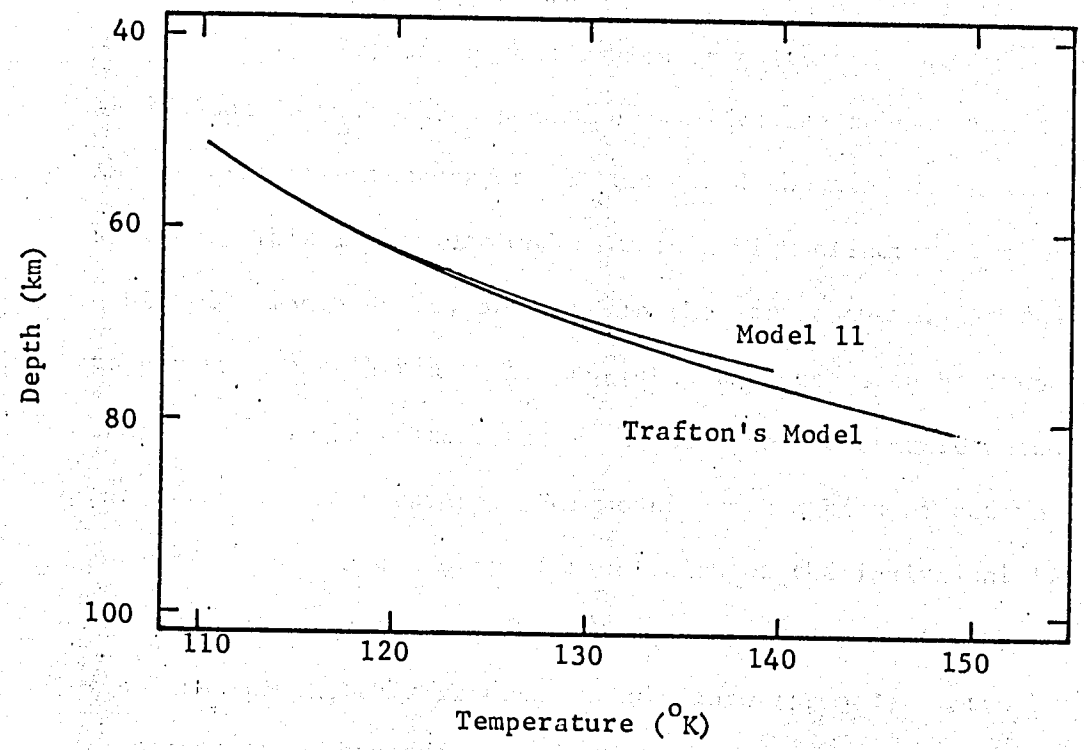

Figure 5.3a

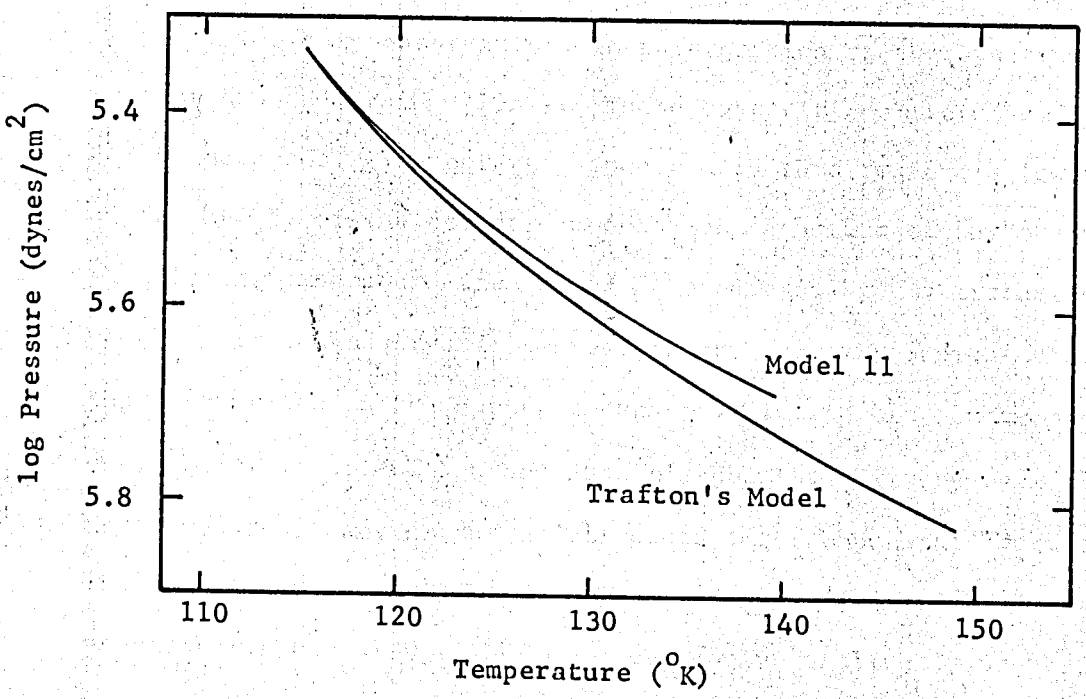

Figure 5.3b
Comparison of Model 11 (Te = 130°K, $\frac{\alpha_2}{\alpha_1} = 0$) with Trafton's model of the same effective Temperature and Composition

.0002, and for models with Te=140°K the lower limit is about .0004.

ii) Inversion Region

The spectrum in this region is quite independent of reasonable variations in α_3. The dependence on effective temperature is rather marked. As the effective temperature is increased the dip becomes much deeper and sharper. This is because models with a high effective temperature contain a bit of ammonia at low pressure in the stratosphere. If the effective temperature was increased beyond 140°K the dip would be even lower, but it could never be lower than the stratospheric temperature which increases with the effective temperature. For models with a high effective temperature, the spectrum plots show a partial resolution of the individual lines making up the inversion spectrum. If the frequency grid used for the calculations was fine enough, this structure would show for models of all effective temperatures. The addition of helium to the models causes a slight increase in the temperature and broadening of the spectrum in this region, but the fine structure appears to remain about the same.

The only observations in this portion of the spectrum are those made by Law and Staelin (1968). These observations are marked in Figure 4.7 by octagons. The observed spectrum in this region is lower than predicted by any of the computed models, and a number of the observations are of a lower temperature than would be predicted by any extension of these models. If the observations are correct, they may indicate that ammonia is super-saturated in the upper atmosphere. Then again, there may be a systematic error in all of Law and Staelin's points. If they were all moved up by the same amount any of the models could fit the points; however, the theoretical spectra for models with a low helium abundance and with effective temperatures near 130°-140°K do seem to give a slightly better fit. The results are not conclusive and further observations are needed. Much

could be gained from a reliable uniformly made set of observations in this wavelength range even if the absolute calibration was not well known.

iii) Long Wavelengths

The spectrum in this region is quite insensitive to the abundance of helium and the dependence on the abundance of ammonia is inseparable from the dependence on effective temperature. The approximate limits which can be placed on these parameters include the limits given by the short wavelength observations and are shown in Figure 5.4.

There is a slight indication that for wavelengths longer than 5 cm., the observed spectrum rises less steeply than the theoretical curves. This possibility is strengthened by the observation by Branson (1968) which gives $250 \pm 40^{\circ}K$ (he agrees [private communication] that this value is probably slightly low) for the disk temperature of Jupiter at 21 cm. Such a flattening could be caused by either an isothermal lower atmosphere at $\sim 270^{\circ}K$, a physical ground at that temperature, or, as suggested by Pollack (1968), strong scattering by ice and water drops which should exist in that region.

An isothermal lower atmosphere could exist only if there was no internal heat source. Even if this was the case, it is debatable whether the isothermal region would be at such a high temperature. The assumption of a ground at this level, where the pressure is less than 10 atmospheres, for a planet composed mostly of hydrogen, is unrealistic. Pollack's hypothesis is quite appealing, and the apparent near-constancy of the microwave temperature at the long wavelengths may be the first observational evidence for the existence of water on Jupiter. The spectrum for model 17 in Figure 4.5 shows the effect that would be produced by adding an optically thick layer at $270^{\circ}K$.

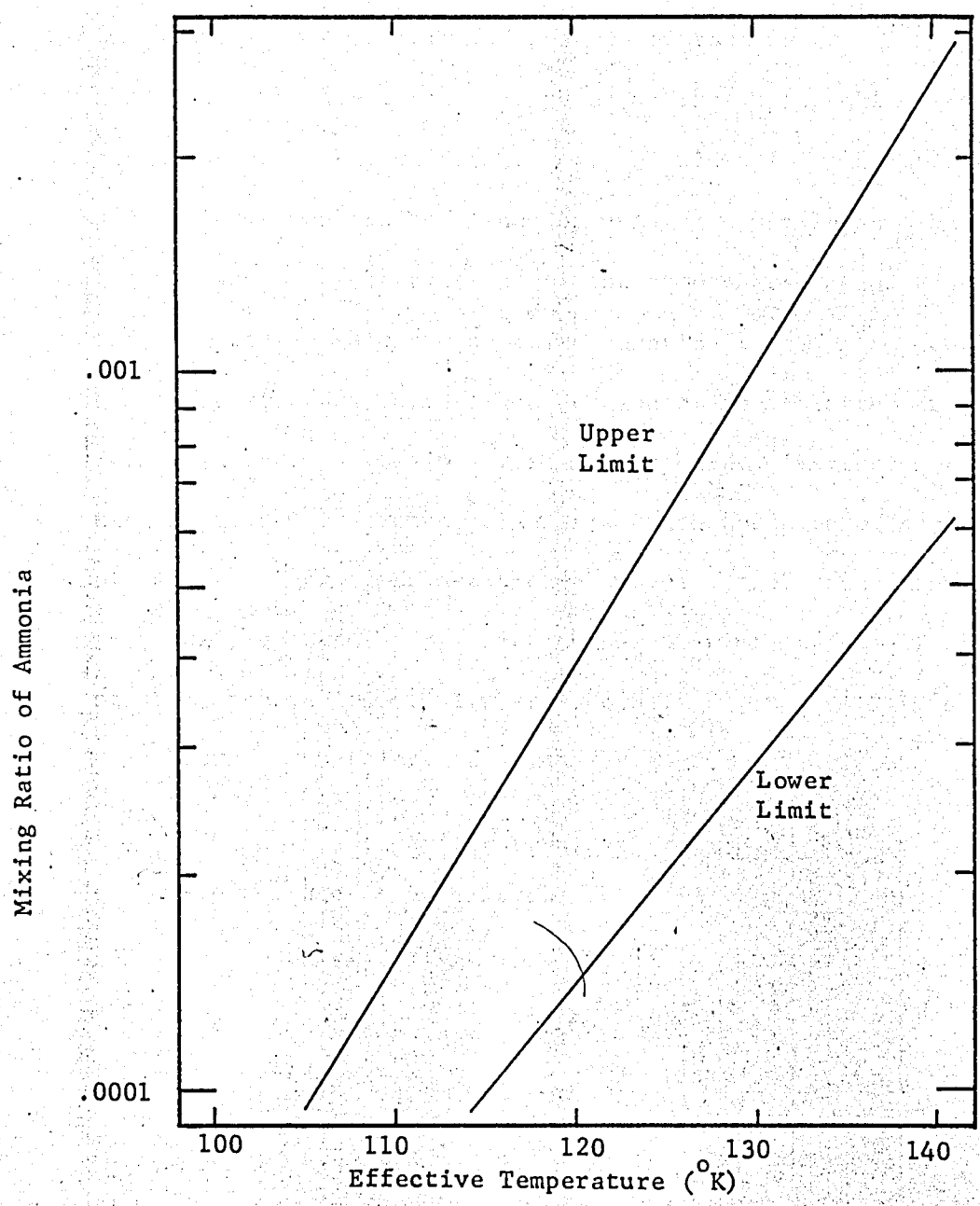

Figure 5.4

Limits for the Mixing Ratio of Ammonia

b) Comparisons of the Models with Other Data

The problem of the scattering of light in the Jovian clouds in the visual and near infrared portion of the spectrum is still, for the most part, unsolved, and this keeps us from being able to calculate the expected equivalent widths of spectral lines for each model. However, some information can be gained by using the models as a basis for comparing the separate observations of the atmospheric abundances, and "cloud-top" temperature and pressure. Absorption lines which are of about the same intensity and in the same portion of the spectrum are probably formed in the same region of the atmosphere. In other words, the quantities deduced from these lines are characteristic of about the same level of the atmosphere. To see the degree of correlation in a qualitative way, the temperatures at which the quantities given in Table 5.2 occur in the various models are shown in Figure 5.5. "Cloud-top" is a vague term which refers to a mean level for reflection of sunlight.

Table 5.2

Characteristic Levels in the Jovian Atmosphere

Top of the Convection Zone	(determined from models)
Cloud Level for Saturated Ammonia	"
700 cm-amagats of NH_3 above the "Cloud-tops"	(inferred from observations--see Introduction)
56 km-amagats of H_2 above the "cloud-top"	"
"Cloud-top" Pressure of 1.6 atmospheres	"
"Cloud-top" Temperature of $\sim 170^{\circ}K$*	

*This value is $10^{\circ}K$ less than the temperature found by Owen and Woodman because their measurement was made at a longer wavelength than any of the others listed in Table 5.2 and thus probably refers to a somewhat deeper level.

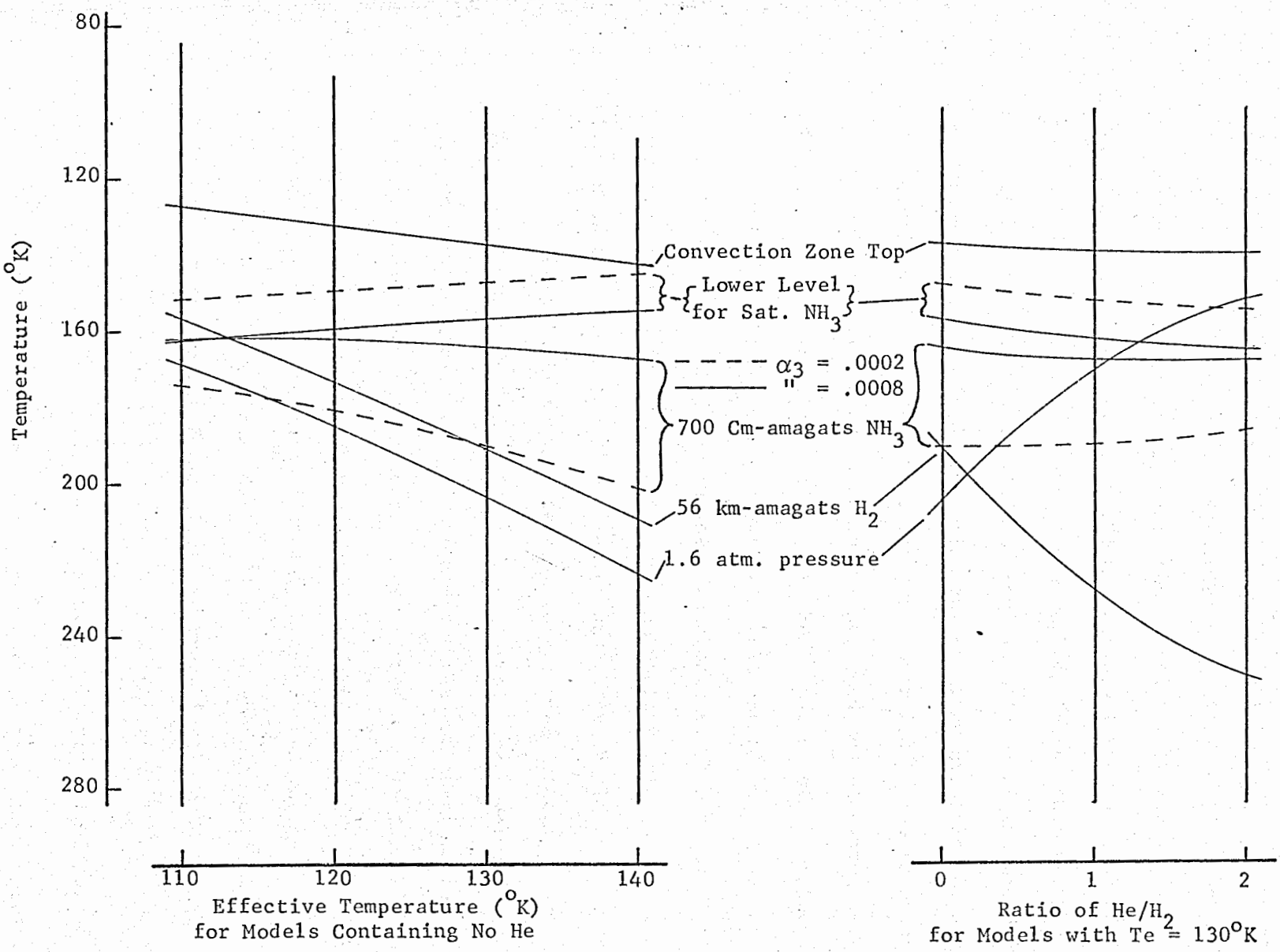

Figure 5.5

Characteristic Levels in Jovian Model Atmospheres

A comparison of Figures 5.4 and 5.5 shows that a model with an effective temperature of about 120°K, containing very little helium, and having an ammonia mixing ratio of about .0002 seems to fit the visual observations and the observations of the microwave brightness temperature. For models with an effective temperature much different than this, a conflict arises between the mixing ratio of ammonia allowed by the microwave spectrum and the ratio deduced from the observed abundance of ammonia. For models with an effective temperature over 130°K, the temperature of the level with the observed pressure and abundance of hydrogen is too high. However, since the theory for the formation of absorption lines in the Jovian cloud layer has not been well worked out, I do not place a great deal of confidence in these conclusions. The theory for the spectrum in the microwave region does not suffer from as many complications as it does in the visual region and these should be more reliable.

The value for the effective temperature deduced by Low and Davidson (1968) of 134 ± 4°K is to be preferred over a value deduced from Figure 5.6 because it is a direct measurement and involved far fewer approximations and assumptions. However, Low has never published in detail his experimental procedure, and his value for the effective temperature is yet to be confirmed by other investigators.

After having considered all of the above results, I feel that the correct parameters for Jupiter are probably close to the following:

$Te \approx 130$°K (strongest weight given to Low and Davidson)

$\frac{\alpha_2}{\alpha_1} \ll 1$ (strongest weight given to Figure 5.5),

$\alpha_3 = .0007 \pm .0004$ (strongest weight given to Figure 5.4), and

$\alpha_5 \sim .003$ (.15 km-amagats of CH_4 and 56 km-amagats of H_2 lie above the same level of the atmosphere.).

5.3 Defense of Assumptions and Cloud Structure

In the construction of the models it was assumed that a) scattering of thermal radiation is negligible, b) the flux is constant throughout the radiative portion of the atmosphere, and c) the atmosphere is in local thermodynamic equilibrium. Now that the most likely parameters for Jupiter have been selected, the validity of these assumptions can be investigated.

a) Scattering and Clouds

Scattering can affect a model only if it occurs in a region of the atmosphere where energy is transferred largely or wholely by radiative processes, i.e., either in the radiative portion of the atmosphere or just a very short way below the top of the convective zone. Rayleigh scattering from molecular hydrogen and helium can be ignored because it is too weak. The scattering coefficient is proportioned to λ^{-4}, and for the region of the Jovian atmosphere being considered, almost all of of the thermal radiation is of longer wavelength than 10μ. Depending upon the model, the quantity of H_2 which lies above the top of the convective zone is between 10 and 30 km-amagats. Using equations from Öpik (1962), it is easy to show that at a wavelength of 10μ the optical depth due to Rayleigh scattering from 30 km-amagats of H_2 is less than 10^{-6}. The possibility of scattering by particles of crystalized ammonia cannot be so assuredly ruled out. Such particles should be formed throughout

that region of the atmosphere which contains saturated ammonia and which is also in convective equilibrium. The quantity and size of these particles probably increases with the vapor pressure of ammonia and the convective velocity. In addition, as was mentioned in the introduction, there is the possibility of a thin layer of particles of solid ammonia lying above the convective zone. Observations have not yet led to many detailed conclusions about the cloud structure.

One of the most apparent aspects of the visible Jovian clouds is that they are divided into a system of bright zones and darker belts. The belts are strongly absorbing in blue light and are much fainter in the infrared. The high contrast between the zones and the belts that is observed in blue light leads to the conclusion that the atmosphere above the cloud deck is quite transparent with very little scattering. The zones show strong limb darkening whereas the belts are of almost uniform intensity across the disk. This, coupled with the observation of Münch and Younkin (1964) that the spectral lines of ammonia and methane appear to be slightly stronger in the zones than in the belts, can be explained by the following hypothesis. Both the zones and the belts are "level" clouds lying at about the same depth in the atmosphere. The difference in brightness probably arises because the scattering albedo is less in the belts than it is in the zones. The cause of this difference may be due to trace amounts of metastable compounds which are distributed in either the upwards or downwards moving convective cells. By "level" it is meant that the mean scattering length is greater than localized vertical variations in the cloud surface. Cumulus-type

clouds, as proposed by Squires (1957), would not give the observed limb darkening. If the clouds had a sharp upper boundary, like our stratus clouds, under a clear atmosphere, the equivalent widths of spectral lines observed near the limb of the planet would be stronger than when observed near the center of the disk. However, if the scattering was uniform, such as would be the case from a uniformly hazy atmosphere, the equivalent widths would decrease towards the limbs. The observed widths of lines in the red and near infrared part of the spectrum are of almost constant width across the disk except near the limbs where they decline slightly (Teifel, 1966; Beckman, 1967). Thus one may infer that the cloud layer neither has a sharp boundary nor does it extend uniformly throughout the whole upper atmosphere. It appears that a model for the clouds consisting of 1) a clear atmosphere overlying, 2) a physically deep but very diffuse, hazy atmosphere, having an optical depth of about one or greater overlying, 3) a sharply bounded reflecting cloud layer might be reasonable. The constancy of the line widths across the disk requires that in the second region the scattering length, measured in terms of quantity of gas, be of the same order of magnitude as the length of the overlying atmosphere. Furthermore, the depth to which light penetrates must be consistent with the observed quantity of gas. Model 11 comes closest to having the proper parameters and is shown in Figure 5.6 to make the discussion more concrete.

The observed temperature and abundance of H_2 are characteristic of levels lying considerably below the top of the convection zone and,

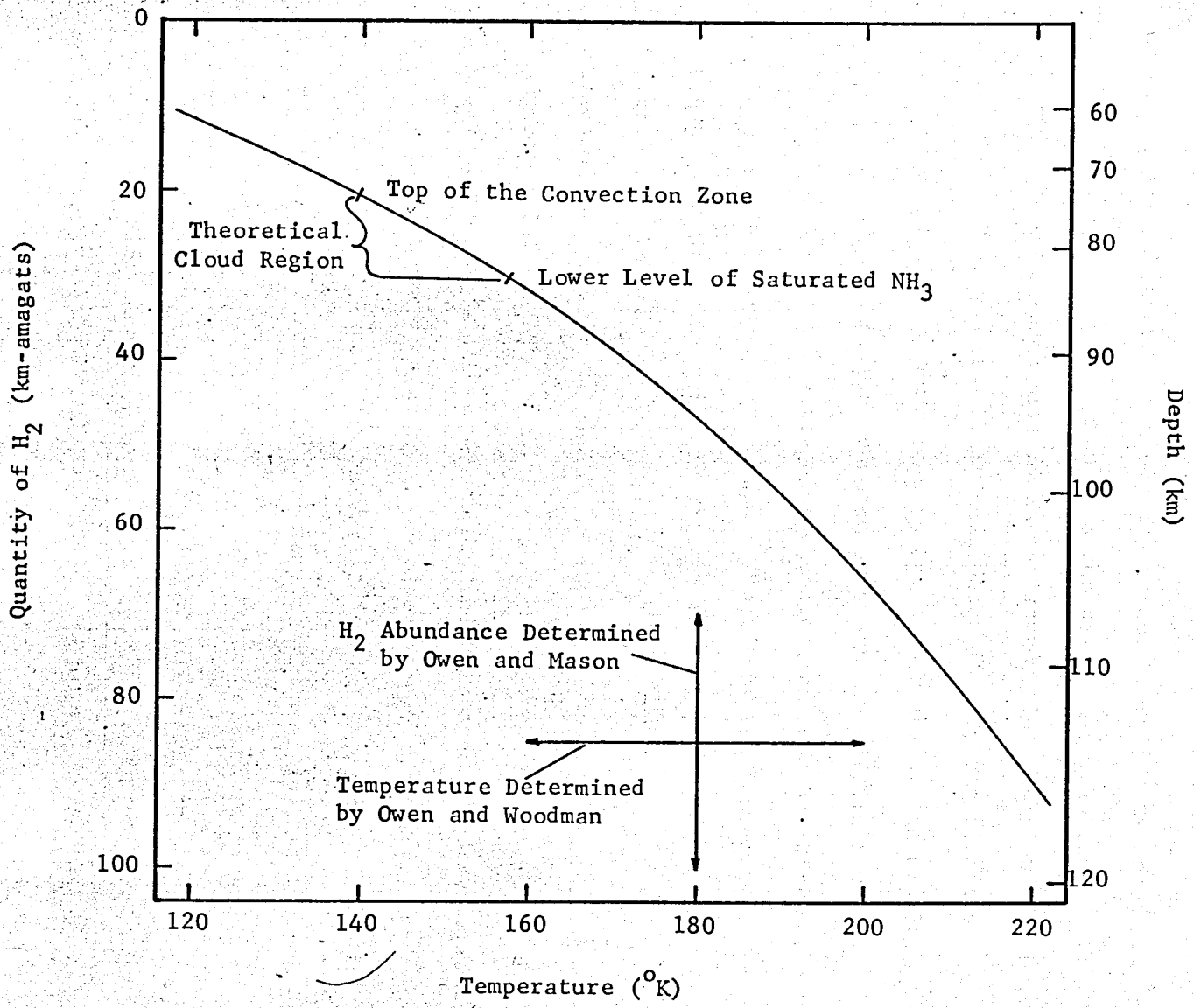

Figure 5.6

Schematic Plot for Model 11 (Te = 130^{o}K, α_2/α_1 = 0, α_3 = .0008)

in fact, even below the theoretical bottom of the ammonia clouds. Two possible explanations are: 1) the thermal opacity used to calculate the models is somewhat in error, and 2) the third (reflecting) layer of clouds is either absent, thin, or scattered. The effect that a change in the thermal opacity would have on the position of the top of the convection zone has been briefly investigated. The position of the top of the convection zone is pretty well determined by the effective temperature and the approximate homology properties of the models. A change in the size of the hydrogen absorption coefficient will change the pressure at the top of the convection zone but will not have any great effect on the temperature. The top of the convection zone is much higher than the reflection level for all reasonable values of effective temperature. As was shown in the preceding section, the position of the theoretical bottom of the cloud layer, in terms of the abundance of H_2, is quite sensitive to the model. Thus it appears that the cloud layer, although probably thickest near its lower surface, is still not optically thick in the red portion of the spectrum. The condition of the scattering length in the hazy cloud region supports this conclusion. If, for example, one assumes that the top of the hazy region starts at the top of the convection zone, then the scattering length should be of the order of 20 km-amagats of H_2 or about 20 km. This length is longer than the theoretical thickness of the cloud layer.

These arguments are all very qualitative and have not been investigated in any more detail than has been presented here. Investigations by various authors have led to almost as many different conclusions. Owen and Mason, who used some of the results of scattering theory suggested that cumulus-type clouds very possibly do exist below the hazy cloud layer. However, their results are still only qualitative, and it would seem that the strong limb darkening observed in the infrared would preclude clouds with strong vertical development. A full accounting of all the observed features connected with the cloud structure is eagerly awaited.

The large scattering length, the apparent slight transparency of the lower clouds coupled with the assumption that the cloud density decreases with the vapor pressure of ammonia leads to the conclusion that the upper clouds must be extremely thin. If a parallel can be drawn between these clouds of frozen particles and our own cirrus clouds, the cloud particles are probably of micron size and smaller. Further evidence for this is the increase in detail seen at longer wavelengths. Considering all of this, it seems quite unlikely that scattering of thermal radiation near the top of the convection zone would be significant.

b) Constancy of Flux

The assumption of the constancy of the thermal flux has been used in the calculation of the radiative gradient. The approximate relationship of the radiative gradient to the flux is given in Eq.(2.27) with $\bar{\kappa}$ given by Eq. (2.6):

$$G_R \propto \frac{P^2}{T^5} \quad . \tag{5.1}$$

The flux has been assumed to come from two sources: an internal source which has been assumed to be constant and uniformly distributed over the entire surface of the planet, and an external source arising from the conversion of solar energy to thermal energy in a deep layer of the atmosphere. The assumptions concerning the first source appear to be quite reasonable, but those concerning the second source must be further investigated.

At some broad level in the atmosphere the incident solar radiation is partially reflected and partially absorbed and converted to thermal energy. Most of this conversion probably occurs in and below the cloud level. About this level the flux is the sum of the fluxes from both sources, but below only the internal source contributes to the total flux. If this decrease in flux were to occur in the radiative zone the radiative gradient would be reduced and the level of convective instability would occur at a deeper level of the atmosphere than originally calculated. If the decrease in flux occurred in the convective region of the atmosphere, it would not affect the models unless the decrease was great enough to return that region to radiative equilibrium. This drastic a decrease in the flux would probably occur only with models which derive most of their heating from the sun (models with $Te \lesssim 120^{\circ}K$). If there is no internal heat source ($Te = 104^{\circ}K$) the deepest layers of the atmosphere must be isothermal. However, Low and Davidson's measurement of the effective temperature indicates that the internal

heating is almost twice as great as solar heating. The application of Eq. (5.1) to Model 11 indicates that convection would be maintained if the amount of solar heating was gradually reduced from its full value at the top of the convection zone to zero at about the 180°K level. This is about the level to which solar radiation penetrates (Owen and Woodman, 1968). The amount of solar radiation which is absorbed above the top of the convection zone is uncertain but is probably quite small considering both the thinness of the clouds and the small amount of pressure broadening of the absorption lines. Thus, for the higher temperature models ($Te \geq 130^{\circ}K$), the flux is probably constant enough for the models to be valid.

c) Assumption of Thermodynamic Equilibrium

Trafton (1967) checked the hypothesis of local thermodynamic equilibrium (LTE) for his models and his results will apply to the models constructed in this thesis as well. He found that LTE does hold in the deeper layers of all the models but deviate towards the surface so that the ratios of absorptions to emissions become as low as .98 for models with $\frac{\alpha_2}{\alpha_1} = 0$ and .93 for models with $\frac{\alpha_2}{\alpha_1} = 1$.

5.4 Suggestions for Future Work

a) Needed Observations

The large errors associated with the available microwave spectrum severely limits the amount of information that can be gained from it even with a careful analysis. Better observations, especially in certain spectral regions, are very much needed. High resolution

spectral scans centered at about 1.26 cm. should be able to lead us to some definite conclusions regarding the temperature of the upper levels of the Jovian atmosphere, even if the absolute calibration of the brightness temperature is uncertain. More observations of the disk temperature of Jupiter at wavelengths longer than 5 cm. are desperately needed, both to better define the thermal spectrum at shorter wavelengths and to confirm the suspicion that the thermal spectrum levels off at about 270°K. Also, an independent direct measurement of Jupiter's effective temperature would be most helpful.

As is discussed in Appendix A, any anomalous dependence with pressure of the line shape of ammonia is expected to be slight for Jovian conditions. However, this has not been experimentally confirmed. Since the microwave spectrum of Jupiter at long wavelengths is quite sensitive to such an effect, the absorption by ammonia in hydrogen and helium at high pressure should be investigated in the laboratory.

b) Further Applications of the Models

At the present time the models are being used to predict the brightness temperature of Jupiter at very high frequency resolution to determine if the individual inversion lines can be resolved sufficiently enough to be observed.

Other investigations which are contemplated are the computation of the brightness temperature and the limb darkening of Jupiter in the far infrared portion of the spectrum.

Appendix A

Description of the Ammonia Molecule

A short description of the ammonia molecule; its energy levels, associated degeneracies, and other quantities which are needed for the computation of the absorption coefficient is given below. Many of the following formulae and much of the development are taken from Townes and Schawlow (1955) without further reference.

The ammonia molecule has the shape of a triangular pyramid with the nitrogen atom located at the top and the three hydrogen atoms located at the three vertices of the equilateral base.

There are six normal modes of vibration, two pairs of which have the same frequency. The vibrational frequencies, ν_i, and the number of modes, g_i, having that frequency are shown in Table A.1.

Table A.1

Vibrational Frequencies

i	$\nu_i (cm^{-1})$	g_i
1	3335	1
2	950	1
3	3414	2
4	1627.5	2

The potential curve of ammonia as a function of the distance between the nitrogen atom and the plane of the hydrogen atoms has a double minimum. This results in a pairing of vibrational levels of opposite parity, i.e. each vibrational level, as listed above, is made up of two inversion levels separated only slightly in energy. The microwave inversion spectrum of ammonia comes from this inversion splitting of the ground vibration state.

The rotational state of the molecule is specified by three rotational constants:

$J = 0, 1, 2, \ldots$

$K = 0, \pm 1, \pm 2, \ldots \pm J$

$M = 0, \pm 1, \pm 2, \ldots \pm J.$

J refers to the total angular momentum, K to its projection on the molecular axis, and M to its projection on an axis fixed in space.

The energy associated with a rotational state is given by

$$E_{J,K} = hc[BJ(J + 1) + (A - B)K^2] \qquad (A.1)$$

where $A = 6.30\ cm^{-1}$, and

$B = 9.94\ cm^{-1}$.

There are other terms in the energy due to centrifugal distortion of the molecule, but they are small and have not been included.

The statistical weight, g, associated with each rotational level is given by

$$g = (2J + 1)g_{IK} \qquad (A.2)$$

where $2J + 1$ is the number of allowed values of M and

g_{IK} is the statistical weight due to spin and K degeneracy.

The Eigenstates of $\pm$ K are degenerate, and the wavefunctions which are antisymmetric with respect to the interchange of two hydrogen nuclei must be formed from a combination of +K and -K states with the appropriate spin functions. Thus properly symmetrized states can be characterized by only the absolute value of K. The value of g_{IK} for each value of $|K|$, from now on designated by only K, and for each separate inversional level is given on Table A.2. The sum of the statistical weights, g_{IK}, over both inversion levels is designated by S(I,K).

Table A.2

Statistical Weights Due to Spin and K Degeneracy

K	g_{IK}
K a multiple of 3 but not 0	4
K not a multiple of 3	2
K = 0, J even, lower inversion level or J odd, upper inversion level	0
K = 0, J odd, lower inversion level or J even, upper inversion level	4

The selection rules for dipole radiation are

$$\Delta J = 0, \pm 1, \quad \Delta K = 0, \text{ and } + \longleftrightarrow - .$$

The last selection rule states that the symmetry of the wave function with respect to inversion about the center of mass must change during a transition. Inversion lines result from transitions in which J = 0, and rotation-absorption lines from transitions in which J = +1. A schematic showing possible absorption lines in the rotation-inversion spectrum of NH_3 is shown in Figure A.1.

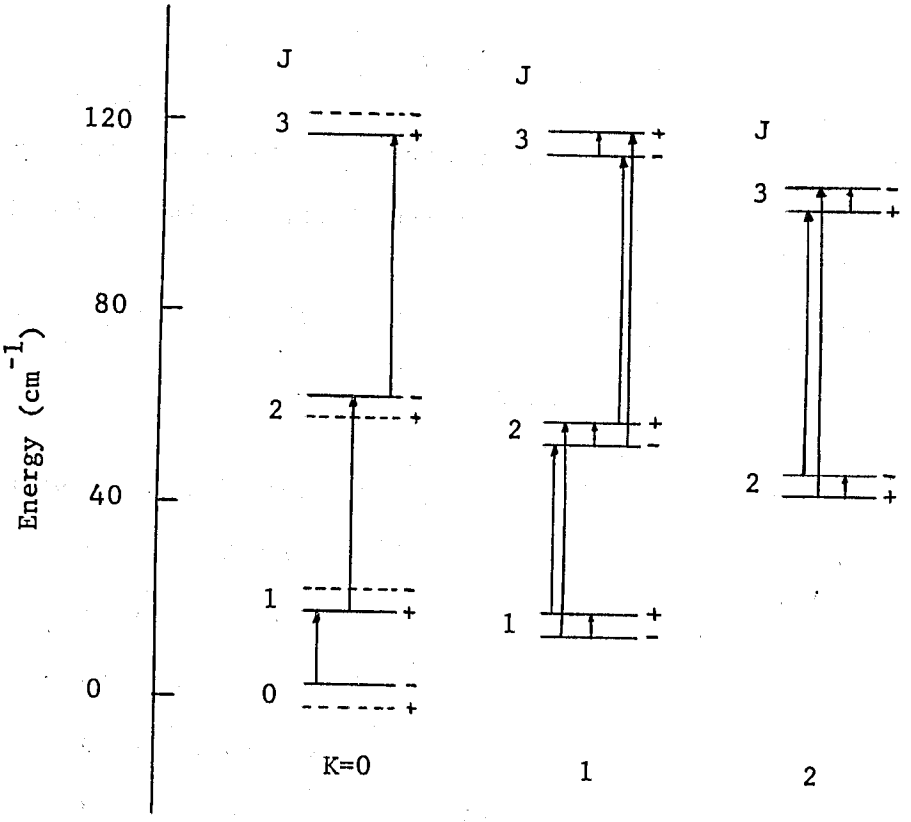

(The inversion splitting has been exaggerated.)

(The statistical weight of levels shown by dashes is zero; therefore they do not exist.)

Figure A.1

Schematic Energy Level Diagram of Ammonia

As can be seen from Figure A.1, except from states for which K = 0, one inversion line, and two rotation lines originate from each rotational level. The two rotation lines differ in frequency by twice the inversion frequency, but this splitting of the rotation lines is so small that it will be ignored.

The frequencies of the rotation lines neglecting the centrifigal distortion terms, are given by

$$\nu_J = \frac{1}{hc} (E_{J+1,K} - E_{J,K}) \approx 2B(J+1) . \qquad (A.3)$$

The frequencies of the inversion lines of the ground vibrational state have been empirically fitted by the formula

$$\nu_{JK} = \nu_o \exp [A'J(J+1) + B'K^2 + C'J^2(J+1)^2 + D'J(J+1)K^2 + E'K^4] + \Delta\nu_{CORR} \qquad (A.4)$$

where $\nu_o = 0.7934101\ (cm^{-1})$,

$A' = -6.36996 \times 10^{-3}$,

$B' = +8.88986 \times 10^{-3}$,

$C' = +8.6922 \times 10^{-7}$,

$D' = -1.7845 \times 10^{-6}$,

$E' = +5.3075 \times 10^{-7}$, and

for $\begin{cases} K \neq 3 & \Delta\nu_{CORR} = 0. \\ K = 3 & \Delta\nu_{CORR} = (-1)^J \cdot 1.167 \times 10^{-8}\ J(J+1)[J(J+1)-2][J(J+1)-6]cm^{-1}. \end{cases}$

This correction gives a good fit to the observed deviations in frequency of the K = 3 lines for the J values 3 through 7, which are strong enough to have been observed. For J > 7, these lines are too weak to have

been observed.

The total monochromatic absorption coefficient is given by

$$\alpha_\nu = \frac{8\pi^3\nu^2}{3}\sum_{J=0}^{\infty}\sum_{K=0}^{J} f_{JK}\left[\frac{1}{hc\nu_{JK}}\left(1-e^{-\frac{hc\nu_{JK}}{kT}}\right)\frac{1}{2}\left|\mu_{JK}\right|^2_{INV} S(\nu,\nu_{JK},\Delta\nu_{JK}) + \right.$$

$$\left. + \frac{1}{hc\nu_J}\left(1-e^{-\frac{hc\nu_J}{kT}}\right)\left|\mu_{JK}\right|^2_{ROT} S(\nu,\nu_J,\Delta\nu'_{JK})\right] \qquad (A.5)$$

where f_{JK} is the fraction of ammonia molecules in the ground vibration state,

and the J, K rotation state, summed over both inversion levels,

$|\mu_{JK}|^2_{INV}$ is the square of the dipole moment matrix element for the inversion transition,

$|\mu_{JK}|^2_{ROT}$ is the square of the dipole moment matrix element for the rotational transition,

$S(\nu,\nu_{JK},\Delta\nu_{JK})$ is the line shape function defined by Eq. A.14,

$\Delta\nu_{JK}$ is the half width of the inversion line originating from the J, K level, and

$\Delta\nu'_{JK}$ is the half width of the rotation line originating from the J, k level.

The first term in Eq. A.5 represents the contribution to the absorption coefficient due to inversion transitions, and the second term due to rotation transitions. There is a factor of ½ in the first term because inversion absorptions can originate from only the lower of the two inversion levels. This factor of ½ is not strictly correct for levels with K = 0, because in this case the statistical weights of the separate inversion levels are not the same--one of the pair has g_{IK} = 0--

so that no inversion transitions can occur. However, this does not cause any error as when $K = 0$, $|\mu_{JK}|^2_{INV} = 0$.

For temperatures which are encountered in the Jovian atmosphere, $hc\nu_{JK} \ll kT$, so the approximation

$$(1 - e^{-\frac{hc\nu_{JK}}{kT}}) = \frac{hc\nu_{JK}}{kT} \tag{A.6}$$

has been made for the inversion lines. For the rotation lines this approximation is not so accurate and has not been made.

The squares of the dipole moment matrix elements are given by

$$\left.\begin{aligned} &\text{for } J+1 \longleftarrow J,\ K \longleftarrow K,\ |\mu_{JK}|^2_{ROT} = \mu^2 \frac{(J+1)^2 - K^2}{(J+1)(2J+1)}, \text{ and} \\ &\text{for } J \longleftarrow J,\ K \longleftarrow K,\ |\mu_{JK}|^2_{INV} = \mu^2 \frac{K^2}{J(J+1)} \end{aligned}\right\} \tag{A.7}$$

where μ is the dipole moment of the ammonia molecule and is equal to 1.468×10^{-18} esu. These are the matrix elements for a molecular transition from a state specified by M to all possible final states specified by M' and are the appropriate elements to be used in Eq. (A.5).

The fractional population of the various energy levels is given by the Boltzmann distribution

$$f_{JK} = F_v \frac{(2J+1)S(I,K)e^{-E_{JK}/kT}}{Q_R} \tag{A.8}$$

where F_v is the fraction of molecules in the vibrational state considered, and Q_R is the rotational partition function given by Eq. (A.11).

The fractional population of the vibrational levels also follows the Boltzmann distribution

$$F_v = \frac{g_v e^{-E_v/kT}}{Q_v} \tag{A.9}$$

where g_v is the statistical weight and is equal to the number of vibration levels which have the same energy. (For ammonia in the ground state $g_v = 1$),

E_v is the energy of vibration relative to the ground state, and

Q_v is the vibrational partition function given by Eq. (A.10).

Thus the fraction of molecules in the ground vibration state is simply $1/Q_v$.

Gordy, Smith and Trambarulo (1953) give expressions for the partition functions. For the vibrational partition function they give

$$Q_v = \prod_i (1-e^{\frac{-hc\nu_i}{kT}})^{-g_i} . \tag{A.10}$$

Calculated values of the vibrational partition function are given in Table A.3.

Table A.3

Vibrational Partition Function of Ammonia

Temp. (^oK)	Q_v
100	1.0000012
150	1.0001106
200	1.0010938
250	1.0044117
300	1.0114377
350	1.0230924
400	1.0398907

As can be seen from the values of Q_v, almost all the ammonia is in the vibrational ground state. For all further calculations I have taken $F_v = 1$ for the ground state.

For an expansion of their expression for the rotational partition function, retaining only the two lowest terms in $\frac{1}{T}$, one obtains

$$Q_R \approx \frac{8}{3}\left[\frac{\pi}{B^2A}\left(\frac{kT}{hc}\right)^3\right]^{\frac{1}{2}}\left[1 + \frac{1}{3}\left(4-\frac{B}{A}\right)\frac{hcB}{4kT}\right] . \tag{A.11}$$

I checked this approximation by comparing its value with the value obtained by doing the sum of the exact formula

$$Q_R = \sum_{J=0}^{\infty}\sum_{K=0}^{J}(2J+1)S(I,K)e^{-\frac{E_{JK}}{kT}} \tag{A.12}$$

up to J = 18. The relative error in the approximation was found to be $< .0005$ at $100^{\circ}K$ and even less at higher temperatures.

Putting Eq. (A.8), (A.9), (A.10), and (A.11) together, one obtains

$$f_{JK} = \frac{3}{8}\left[\frac{B^2A}{\pi}\left(\frac{hc}{kT}\right)^3\right]^{\frac{1}{2}}\left[1 + \frac{1}{3}\left(4-\frac{B}{A}\right)\frac{hcB}{4kT}\right]^{-1}(2J+1)S(I,K)e^{-\frac{E_{JK}}{kT}} \tag{A.13}$$

where

$$S(J,K) = \begin{cases} 4 & \text{if } K = 0 \\ 4 & \text{if } K \text{ is not a multiple of 3} \\ 8 & \text{if } K \text{ is a multiple of 3 but not 0.} \end{cases}$$

The line-shape and half-widths have been obtained from a combination of theoretical and empirical results. Anderson (see Townes and Schawlow, section 13-8) has given a rather good treatment of pressure broadening. For the line-shape, he gets

$$S(\nu,\nu_o,\Delta\nu) = \frac{1}{\pi}\left[\frac{\Delta\nu}{(\nu-\nu_o-a\Delta\nu)^2+(\Delta\nu)^2} + \frac{\Delta\nu}{(\nu+\nu_o+a\Delta\nu)^2+(\Delta\nu)^2}\right] . \qquad (A.14)$$

The frequency shift, $a\Delta\nu$, is usually negligible for microwave frequencies. When $a = 0$, this reduces to the familiar VanVleck-Weisskopf line-shape.

The half-widths depend upon what type of molecule is colliding with the ammonia, the pressure, the temperature, and the rotational state of the ammonia molecule as specified by J and K.

During a collision between two ammonia molecules there is a strong dipole-dipole interaction. The interaction between ammonia molecules and hydrogen or helium molecules is much weaker as evidenced by their smaller effective diameters (see Townes and Schawlow, Table 13-4), and is of the quadrapole-induced dipole type.

At low densities, in which two body collisions predominate, the interaction energy between the two colliding molecules has the form $\frac{1}{r^n}$, and

$$\Delta\nu \propto PT^{-(n+1)/2(n-1)} \qquad (A.15)$$

$n = 3$ for dipole-dipole interactions

$n = 7$ for quadrapole-induced dipole interactions.

For NH_3-NH_3 collisions the widths of many of the inversion lines have been carefully measured, and an empirical formula by Bleaney and Penrose (Townes and Schawlow, Eq. 13-61) has been found to give a good fit.

For collisions between ammonia and other molecules, the measurements have not been so extensive, so I have had to rely on a theoretical formula by Anderson (Townes and Schawlow, Eq. 13-60) to get the functional form of the line width dependence on J and K for n = 7 type collisions.

The proportionality constants in Eqs.(A.16) have been determined from the measured line widths of the J = 3, K = 3 inversion line for broadening by various gases (Townes and Schawlow, Table 13-4).

The results for the half-widths of the ammonia inversion lines are:

For NH_3 broadening*

$$\Delta\upsilon_{NH_3} = C_{NH_3} \frac{P_{NH_3}}{T} \left[\frac{K^2}{J(J+1)}\right]^{\frac{1}{3}} \qquad \text{(A.16a)}$$

For H_2 and He broadening

$$\Delta\upsilon_{H_2,He} = \begin{Bmatrix} C_{H_2} \\ C_{He} \end{Bmatrix} \frac{P_{H_2,He}}{T^2/3} \left\{\frac{K^2}{J(J+1)} \left[1+\frac{22}{5}\frac{K^2}{J(J+1)}+\frac{121}{5}\frac{K^4}{J^2(J+1)^2}\left(\frac{22}{5}+\frac{121}{7}\frac{K^2}{J(J+1)}\right) + \right.\right.$$

$$\left.\left. + \frac{121}{63}\frac{K^4}{J^4(J+1)^4}\right]\right\}^{1/6} \qquad \text{(A.16b)}$$

*The subscript represents the type of molecule colliding with the ammonia molecule.

where $C_{NH_3} = 2.90 \times 10^{-1}$ cm^{-1}°K/mmHg,

$C_{He} = 1.44 \times 10^{-3}$ cm^{-1}°K$^{2/3}$/mmHg,

$C_{H_2} = 3.33 \times 10^{-3}$ cm^{-1}°K$^{2/3}$/mmHg, and

P_{NH_3}, P_{H_2}, and P_{He} are the partial pressures of ammonia, hydrogen and helium, respectively.

When pressure broadening is due to more than one constituent, the half-widths due to each one are added, i.e.

$$\Delta\nu_{TOTAL} = \Delta\nu_{NH_3} + \Delta\nu_{H_2} + \Delta\nu_{He} \cdot \qquad (A.17)$$

I have found no high resolution measurements for the half-widths of the ammonia rotation lines so I have resorted to an approximate theory. The broadening of the line may be considered to arise from transitions between levels which have been statistically broadened by collisions. For collisional broadening and natural broadening, the half-width of a spectral line is just the sum of the half-widths of the two levels which the line connects.

If one makes the assumption that both inversion levels of a given rotational level are broadened equally, then the conclusion is that each inversion level has a width of one half the widths of the inversion line which arises between them. I have made this assumption. Then, since a rotation line connects a level, J, K, with a level, J + 1, K, its half width is given by

$$\Delta\nu'_{JK} = \frac{1}{2}(\Delta\nu_{JK} + \Delta\nu_{J+1,K}) \cdot \qquad (A.18)$$

The preceding formulae have been developed for ammonia at "low pressures." Bleaney and Loubser (1950) have observed the spectrum of pure ammonia at pressures ranging up to 6 atmospheres. They have noted the following:

1. $\frac{\Delta\nu}{p}$ initially decreased almost linearly with pressure and then reached a constant value about $\frac{1}{3}$ as much as the initial value.
2. The central frequency of the inversion line varied with pressure being nearly constant with a value of ~ 8 cm^{-1} at low pressures and dropping rapidly to 0 cm^{-1} for pressures above 2 atmospheres.

These changes are shown graphically in Figure A.2 which is a reproduction of Bleaney and Loubser's Figure 3.

Figure A.2

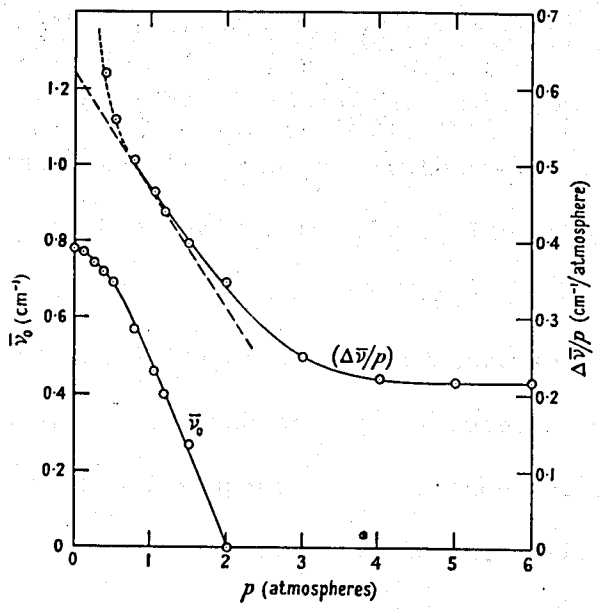

Figure 3. Variation with pressure of apparent inversion frequency, $\bar{\nu}_0$, and line width per atmosphere, $\Delta\bar{\nu}/p$, for ammonia.

The change in the inversion frequency is apparently caused by the strong dipole-dipole interaction that exists between ammonia molecules when they are close together. Since the quadrapole-induced dipole interaction is considerably weaker, the effect should be much less for small quantities of ammonia in hydrogen-helium mixtures.

For lack of any definite information, I have assumed that the density at which a given frequency shift occurs is inversely proportional to the cube of the collision diameters. Using the collision diameters for microwave absorption as given in Townes and Schawlow, Table 13-4, the pressure required to produce a given frequency shift for ammonia in hydrogen is 91 times as great as for pure ammonia. For ammonia in helium the pressure needed is 195 times as great as for pure ammonia. An inspection of Figure A.2 will show that the change in the central frequency is very small for pressures less than 30 cm Hg. in pure ammonia. If I assume that $\nu_o \approx$ constant for pressures up to 30 cm Hg. (at 293°K) in pure ammonia, then this approximation should be good for pressures up to 37.5 atmospheres (at 293°K) for ammonia in hydrogen and for even higher pressures for ammonia in helium. This is greater than any of the densities encountered in the models.

Bleaney and Loubser explain the fall of the value of $\frac{\Delta\nu}{P}$ in the following way. The actual diameter of an ammonia molecule is smaller than the effective collision diameter for microwave absorption for NH_3-NH_3 collisions. Thus an absorbing molecule, A, will have a colliding molecule, B, within its sphere of influence for a certain fraction, f, of the total time. If another molecule, C, collides with A during

this time, the collision is not effective in contributing to the line width since the absorption of radiation was already interrupted. Thus only molecules which have no other molecules already in their sphere of influence can contribute to line broadening. If f′ is the fraction of time that no other molecules are in the sphere of influence of molecule A, we can write

$$\frac{\Delta\nu}{P} = f'\left(\frac{\Delta\nu}{P}\right)_{P=0} .$$

For NH_3-H_2, and NH_3-He collisions, the effective collision diameters for microwave absorption are smaller than the kinetic theory collision diameters so the volume of the sphere of influence must be extremely small, and I believe the result would be no change in the value of $\frac{\Delta\nu}{P}$ until extremely high pressures are reached.

In line with the above arguments, I have ignored including any high-pressure effects in the spectrum of ammonia, and thus I have taken "a" in Eq. (A.14) to be zero.

The various terms in the ammonia absorption coefficient can no be collected together from Eqs.(A.1), (A.5), (A.6), (A.7) and (A.13).

$$\alpha_\nu = \frac{\pi^3\mu^2}{kT}\left[\frac{B^2A}{\pi}\left(\frac{hc}{kT}\right)^3\right]^{\frac{1}{2}}\left[1+\frac{1}{3}\left(4-\frac{B}{A}\right)\frac{hcB}{4kT}\right]^{-1}\nu^2\sum_{J=0}^{\infty}\sum_{K=0}^{J}(2J+1)S(I,K)e^{-hc[BJ(J+1)-}$$

$$-(A-B)K^2]/kT \times\left\{\frac{1}{2}\frac{K^2}{J(J+1)}S(\nu,\nu_{JK},\Delta\nu_{JK}) + \frac{kT}{hc\nu_J}\left(1-e^{-\frac{hc\nu_J}{kT}}\right)\frac{(J+1)^2-K^2}{(J+1)(2J+1)}\right.$$

$$\left.S(\nu,\nu_J,\Delta\nu'_{JK})\right\} \qquad (A.19)$$

Numerically, this is

$$\alpha_\nu(\mathrm{cm}^2) = 1.175894 \times 10^{-17}\left[1+\frac{2.8868257}{T}\right]^{-1} \frac{1}{T^{5/2}}\, \nu^2 \sum_{J=0}^{\infty} \sum_{K=0}^{J} (2J+1)$$

$$S(I,K)\, e^{-[9.94J(J+1)-3.64K^2]/0.695022T} \times \left\{ \frac{1}{2} \frac{K^2}{J(J+1)} S(\nu, \nu_{JK}, \Delta\nu_{JK}) + \right.$$

$$\left. + \frac{0.695022T}{\nu_J}\left(1-e^{-\frac{\nu_J}{0.695022T}}\right)\frac{(J+1)^2-K^2}{(J+1)(2J+1)} S(\nu, \nu_J, \Delta\nu'_{JK}) \right\}$$

where

$$S(I,K) = \begin{cases} 4 & \text{if } K = 0 \\ 4 & \text{if } K \text{ is not a multiple of 3} \\ 8 & \text{if } K \text{ is a multiple of 3 but not 0.} \end{cases}$$

The line shape is taken from Eq. (A.14) with "a" equal to zero

$$S(\nu, \nu_o, \Delta\nu) = \frac{1}{\pi}\left[\frac{\Delta\nu}{(\nu-\nu_o)^2} + \frac{\Delta\nu}{(\nu+\nu_o)^2+\Delta\nu^2}\right]. \qquad (A.20)$$

The line frequencies are given by Eqs. (A.3) and (A.9), and the half widths by (A.17) and (A.18)

$$\Delta\nu_{JK} = \Delta\nu_{NH_3} + \Delta\nu_{H_2} + \Delta\nu_{He} \qquad (A.17)$$

$$\Delta\nu'_{JK} = \frac{1}{2}(\Delta\nu_{J,K}+\Delta\nu_{J+1,K}) \qquad (A.18)$$

where $\Delta\nu_{NH_3}$, $\Delta\nu_{H_2}$, and $\Delta\nu_{He}$ are given by Eq. (A.16).

Appendix B

Water Vapor Absorption at Microwave Frequencies

The water molecule, like the ammonia molecule, has a large dipole moment. Thus the interactions between a water molecule and other molecules are expected to be similar to those between an ammonia molecule and other molecules, especially in regard to collisional line broadening.

The water vapor absorption coefficient, $\varkappa_w$, is composed of two terms: $\varkappa_w = \varkappa_{w1} + \varkappa_{w2}$. $\varkappa_{w1}$ is the absorption introduced by an electric dipole resonance centered at 22235.22 mHz = 0.74 cm^{-1} (NBS Circular 518, 1952). It is the largest term for frequencies near 1 cm^{-1} and at low pressures. Additional absorption, represented by the coefficient $\varkappa_{w2}$, is introduced by the strong water vapor resonances in the infrared, the skirts of which exhibit a significant effect even at microwave frequencies. The strongest of these bands is centered at a frequency of about 150 cm^{-1} (Allen, 1963). At high pressures, where the line width is large, the second term is the largest.

The water vapor absorption coefficient can be written in the same form as the ammonia absorption coefficient, see Eq.(A.5).

$$\varkappa_w = N_{H_2O}\{A_1(T)\frac{1}{hc\nu_1}(1-e^{-\frac{hc\nu_1}{kT}})S(\nu,\nu_1,\Delta\nu_1)+A_2(T)\frac{1}{hc\nu_2}(1-e^{-\frac{hc\nu_2}{kT}})S(\nu,\nu_2,\Delta\nu_2)\}\nu^2 \qquad (B.1)$$

where κ_w is the absorption coefficient (cm^{-1}),

$A_1(T)$ and $A_2(T)$ are functions of temperature related to the populations of the various levels multiplied by their respective dipole moment matrix elements,

$$S(\nu,\nu_i\Delta\nu_i) = \frac{\Delta\nu_i}{(\nu-\nu_i)^2+\Delta\nu_i^2} + \frac{\Delta\nu_i}{(\nu+\nu_i)^2+\Delta\nu_i^2}\ ,^{*} \qquad (B.2)$$

$$\nu_1 = 0.74\ cm^{-1}\ , \quad \text{and}$$

$$\nu_2 = 150\ cm^{-1}\ .$$

The following approximations are now made with negligible error: at Jovian temperatures

$$(1-e^{-\frac{hc\nu_2}{kT}}) = \frac{hc\nu_2}{kT}\ ,$$

$$\Delta\nu_2 \ll \nu_2 \quad \text{(Hogg, 1959)}$$

and at microwave frequencies $\nu \ll \nu_2$, therefore

$$S(\nu_1,\nu_2,\Delta\nu_2) = \frac{2\Delta\nu_2}{\nu_2^2} = \frac{2\Delta\nu_2}{150^2}\ .$$

With these approximations, and with the equation $P_{H_2O}\ (mmHG) = 760\ \frac{N_{H_2O}}{L_o}\ \frac{T}{273}$, the absorption coefficient can be written

---

*Note that S as defined here is π times S as defined by Eq. (A.14) and used for ammonia.

$$\kappa_w = \frac{L_o}{273k}\left(\frac{P_{H_2O}}{760}\right)\left(\frac{273}{T}\right)^2 \{A_1(T)\left[\frac{\Delta\nu_1}{(\nu-.74)^2+\Delta\nu_1^2} + \frac{\Delta\nu_1}{(\nu+.74)^2+\Delta\nu_1^2}\right] + \\ + \frac{k}{hc}\frac{T}{150}\left(1-e^{-\frac{hc}{k}\frac{150}{T}}\right)A_2(T)\frac{2\Delta\nu_2}{150^2}\}\nu^2 \quad . \tag{B.3}$$

This equation can be made to appear simpler by defining factors

$$B_1(T) = \frac{L_o}{273k}\frac{A_1(T)}{760} \text{ and } B_2(T) = \frac{L_o}{273k}\frac{k}{hc}\frac{T}{150}\left(1-e^{-\frac{hc}{k}\frac{150}{T}}\right)\frac{A_2(T)}{760} \quad . \tag{B.4}$$

Townes and Schawlow (page 346) show a graph of the water vapor microwave spectrum in the frequency region centered at 0.75 cm^{-1}. Their spectrum is for 10.2 mmHg water vapor in air at 293°K and 760 mmHg pressure.

Eq. (B.3) was fitted to the experimental results by taking the experimental values at three frequencies as shown in Table B.1.

Table B.1

Values of the Water Vapor Absorption Coefficient for 10.2 mmHg. Water Vapor in Air at 293°K and 760 mmHg Pressure.

ν[gHz]	ν[cm^{-1}]	κ_w[cm^{-1}]
17.5	0.853	1.14×10^{-7}
22.5	0.750	5.76×10^{-7}
40.0	1.333	2.47×10^{-7}

The results are as follows:

$$\Delta\nu_1 = 0.090 \text{ cm}^{-1} \text{ (Hogg says } \Delta\nu_1 = 0.1 \text{ cm}^{-1}),$$

$$B_1(293) = 0.91 \times 10^{-8} \text{ mmHg}^{-1},$$

$$B_2(293)\frac{2\Delta\nu_2}{150^2} = 1.316 \times 10^{-8} \text{ cm/mmHg}.$$

Thus the absorption coefficient can be written

$$\kappa_w = P_{H_2O}\left(\frac{273}{T}\right)^2 \{0.91\times10^{-8}\frac{B_1(T)}{B_1(293)}\left[\frac{\Delta\nu_1}{(\nu-.74)^2+\Delta\nu_1^2} + \frac{\Delta\nu_1}{(\nu+.74)^2+\Delta\nu_1^2}\right] + 1.316\times10^{-8}\frac{B_2(T)}{B_2(293)}\frac{\Delta\nu_2}{\Delta\nu_{20}}\}\nu^2 \qquad (B.5)$$

where $\Delta\nu_{20}$ is the value of $\Delta\nu_2$ at the experimental conditions.

From Townes and Schawlow (page 368) one finds that $\Delta\nu \propto PT^{-\frac{n+1}{2(n-1)}}$. For collisions between molecules without a permanent dipole moment with a water molecule n = 7, so $\Delta\nu \propto PT^{-2/3}$. Thus the equations for the line widths can be written as

$$\Delta\nu = \left(\frac{P}{760}\right)\left(\frac{273}{T}\right)^{2/3}\Delta\nu_{N_2}\left[\alpha_{N_2} + \frac{\Delta\nu_{O_2}}{\Delta\nu_{N_2}}\alpha_{O_2} + \frac{\Delta\nu_{H_2}}{\Delta\nu_{N_2}}\alpha_{H_2} + \frac{\Delta\nu_{He}}{\Delta\nu_{N_2}}\alpha_{He} + \text{etc.}\right] \qquad (B.6)$$

where α_i is the molar fraction of the i^{th} component and

$\Delta\nu_{N_2}$ is the line width produced by collisions between nitrogen molecules and water molecules at S.T.P.

Another assumption that must now be made is that the relative sizes of line widths produced by collisions between water and other molecules is probably about the same as it is for collisions between ammonia and other molecules. Thus $\left(\frac{\Delta\nu_i}{\Delta\nu_{N_2}}\right)_{\text{water}} = \left(\frac{\Delta\nu_i}{\Delta\nu_{N_2}}\right)_{\text{ammonia}}$. This assumption seems reasonable as both water molecules and ammonia molecules have strong dipole moments, and the manner in which they interact with other molecules is, therefore, probably similar. In Townes and Schawlow (page 363) the line widths produced by collisions between ammonia and other molecules can be found. From their Table 13-4, the following ratios were calculated:

$$\frac{\Delta\nu_{O_2}}{\Delta\nu_{N_2}} = 0.605, \quad \frac{\Delta\nu_{H_2}}{\Delta\nu_{N_2}} = 0.790, \quad \frac{\Delta\nu_{He}}{\Delta\nu_{N_2}} = 0.342 \ . \qquad \text{(B.7)}$$

The value of $\Delta\nu_{N_2}$ can be determined for the line centered at 0.74 cm^{-1} with the aid of Eq. (B.6) and (B.7), and from the known width of this line, 0.090 cm^{-1}, at the experimental conditions: P = 760 mmHg, T = 293°K, $\alpha_{N_2} = 0.8$, $\alpha_{O_2} = 0.2$. The result is $\Delta\nu_{N_2} = 0.1025$ cm^{-1}.

Although the value of $\Delta\nu_{N_2}$ for the line centered at 150 cm^{-1} cannot be determined because the experimental line width was not measured, the value of $\frac{\Delta\nu_2}{\Delta\nu_{20}}$ can be determined for this line also with the aid of Eq. (B.5) and (B.6), and the experimental conditions.

The resulting equations for the line widths and absorption coefficient are

$$\Delta\nu_1 = 0.1\left(\frac{P}{760}\right)\left(\frac{273}{T}\right)^{2/3}\left[1.025\alpha_{N_2}+0.620\alpha_{O_2}+0.810\alpha_{H_2}+0.350\alpha_{He}\right], \tag{B.8}$$

$$\frac{\Delta\nu_2}{\Delta\nu_{20}} = 11.09\Delta\nu_1 \text{ , and} \tag{B.9}$$

$$\kappa_w = P_{H_2O}\left(\frac{273}{T}\right)^2\left\{0.91\times10^{-8}\,\frac{B_1(T)}{B_1(293)}\left[\frac{\Delta\nu_1}{(\nu-.74)^2+\Delta\nu_1^2}+\frac{\Delta\nu_1}{(\nu+.74)^2+\Delta\nu_1^2}\right]+\right.$$

$$\left.+\,14.59\times10^{-8}\frac{B_2(T)}{B_2(293)}\,\Delta\nu_1\right\}\nu^2 . \tag{B.10}$$

This formula can be evaluated only at 293°K. At other temperatures the functions $\frac{B_1(T)}{B_1(293)}$ and $\frac{B_2(T)}{B_2(293)}$ are not known. Fortunately, however, this same temperature falls in the middle of the temperature range of those layers in the Jovian atmosphere in which the existence of water vapor could cause an observable effect in the microwave spectrum of Jupiter. For temperatures below about 250°K the vapor pressure of water becomes negligible, and only a very small fraction of the radiation originating in layers hotter than about 330°K reaches the surface without being reabsorbed.

Ho, Kaufman, and Thaddeus (1966) also made measurements of the microwave absorption coefficient of water vapor. They made their observations at a single frequency, 0.324 cm^{-1}, at temperatures from 393°K to 473°K, and at high pressures ranging up to 130 atm. in N_2. Their results were fitted to a semi-empirical formula, which in my notation is

$$\kappa_w = 1.75 \times 10^{-8} P_{H_2O} \left(\frac{273}{T}\right)^5 \left(\frac{P}{760}\right) \nu^2 (cm^{-1}). \qquad (B.11)$$

This equation is valid only at pressures high enough that the contribution to the absorption coefficient from the 0.74 cm^{-1} line can be ignored.

A comparison of the values for the absorption coefficient as predicted by Eq. (B.10) with that predicted by Eq. (B.11) was made. This comparison was made for a case for which both equations could be applied, T = 293°K, P = 50 atm, $\alpha_{N_2} = 1$, $\nu = 0.324$ cm^{-1}. For these conditions the results of the two equations agree with each other within 1%. At these conditions, the contribution by κ_{w1} to the total absorption coefficient is only 0.5%, thus Eq. (B.10) can be approximately written as

$$\kappa_w = 14.59 \times 10^{-8} (0.1025) P_{H_2O} \left(\frac{273}{T}\right)^{8/3} \frac{B_2(T)}{B_2(293)} \left(\frac{P}{760}\right) \nu^2 \ (cm^{-1}) \ .$$

From a comparison of this equation with Eq. (B.11), it can be seen that

$$\frac{B_2(T)}{B_2(293)} \approx \left(\frac{293}{273}\right)^{7/3} \left(\frac{273}{T}\right)^{7/3} = 1.179 \left(\frac{273}{T}\right)^{7/3} . \qquad (B.12)$$

I have assumed that the function $\frac{B_1(T)}{B_1(293)}$ is the same as $\frac{B_2(T)}{B_2(293)}$ although this has not been determined. The error that results in making this assumption is probably quite small, because for the conditions of interest in the Jovian atmosphere the temperature is near 293°K and κ_{w1} is only about 20% of κ_{w2}.

With these approximations, the absorption coefficient can be written

$$\kappa_w = P_{H_2O}\left(\frac{273}{T}\right)^{13/3}\nu^2\{1.073\times10^{-8}\left[\frac{\Delta\nu_1}{(\nu-.74)^2+\Delta\nu_1^2}+\frac{\Delta\nu_1}{(\nu+.74)^2+\Delta\nu_1^2}\right]+$$

$$+ 17.20\Delta\nu_1\} . \qquad \text{(B.13)}$$

A comparison of the microwave absorption on Jupiter due to water vapor and due to ammonia can now be made. The water vapor absorption is determined with Eq. (B.13) and the ammonia absorption is obtained from computer output through Eq. (A.19).

The comparison is made at a level in the atmosphere having a temperature of 273°K and at a frequency of 0.4 cm^{-1}. If it is assumed that at this level water vapor is saturated then it is at its vapor pressure of 4.579 mmHg. The partial pressure of ammonia depends on the atmospheric model chosen. A value between 1 and 5 mmHg seems reasonable so I will assume that the partial pressures (or concentrations) of ammonia and water vapor are equal. For the model Te = 120°K, $\alpha_1 = 0.5$, $\alpha_2 = 0.5$, the total pressure at the 273°K level is about 6500 mmHg.

Under these conditions, i.e., T = 273°K, P = 6500 mmHg, $\alpha_1 = 0.5$, $\alpha_2 = 0.5$, $P_{H_2O} = 1$ mmHg, $P_{NH_3} = 1$ mmHg, $\nu = 0.4$ cm^{-1}, the absorption coefficients are

$$\kappa_{NH_3} = 2.63\times10^{-6} \ (cm^{-1}), \quad \text{and}$$

$$\kappa_{H_2O} = 1.66\times10^{-8} \ (cm^{-1}) \ (18\% \text{ of which comes from the } 0.74 \ cm^{-1} \text{ line}).$$

Thus for equal concentrations of water vapor and ammonia, water vapor contributes 0.63% to the absorption coefficient. At longer wavelengths this ratio remains about the same since the absorption coefficient is approximately proportional to ν^2 for both of these gases. The conclusion is that H_2O can be disregarded as a significant absorber in the Jovian atmosphere.

REFERENCES

Allen, C. W. 1963, Astrophysical Quantities (2d ed.; London: Athlone Press).

Aller, L. H. 1963, The Atmospheres of the Sun and Stars (2d ed.; New York: Ronald Press Co.).

American Petroleum Institute Research Project 44, Serial 528, 1946, (Washington, D. C.: National Bureau of Standards).

————, Serial 1713, 1955 (Washington, D.C.: National Bureau of Standards).

Badger, R. M., and Cartwright, C. H. 1929, Phys. Rev., 33, 692.

Baum, W. A., and Code, A. D. 1953, A. J., 58, 108.

Beckman, J. E. 1967, Ap. J., 149, 453.

Berge, G. L. 1966, Ap. J., 146, 767.

Bibinova, V. P., Kuzmin, A. D., and Salomonovich, A. E. 1962, Soviet Astr.-AJ, 6, 840.

Bishop, E. V., and DeMarcus, W. C. 1968, paper presented at the 128th meeting Am. Astr. Soc., Austin, Texas, December 10, 1968.

Bleaney, B., and Loubser, J. H. N. 1950, Proc. Phys. Soc., 63, 483.

Branson, N. J. B. A. 1968, M. N. R. A. S., 139, 155.

Burch, D. E., Singleton, E. B., and Williams, D. 1962, Appl. Opt., 1, 359.

Burch, D. E., and Williams, D. 1962, Appl. Opt., 1, 587.

Danielson, R. E. 1966, Ap. J., 143, 949.

Dickel, J. R. 1964, unpublished Ph.D. Thesis, University of Michigan.

————, 1967a (private communication).

————, 1967b, Ap. J. 148, 535.

Dickel, J., Degioanni, J., and Goodman, G. 1969 (in preparation).

Epstein, E. E. 1968, Ap. J., 151, L149.

Field, G. B. 1959, J. Geophys. Res., 64, 1169.

Foley, H. M., and Randell, H. M. 1941, Phys. Rev., 59, 171.

France, W. L., and Williams, D. 1966, J. Opt. Soc. Am., 56, 70.

Garing, J. S., Nielsen, H. H., and Rao, K. N. 1959, J. Mol. Spect., 3, 496.

Giordmaine, J. A., Alsop, L. E., Townes, C. H., and Mayer, C. H. 1959, A. J., 64, 332.

Gordy, W., Smith, W. V., and Trambarulo, R. F. 1953, Microwave Spectroscopy (New York: John Wiley and Sons).

Greenspan, J. A., and Owen, T. 1967, Science, 156, 1489.

Gross, S. H. and Rasool, S. I. 1964, Icarus, 3, 311.

Handbook of Chemistry and Physics 1954 (36th ed.; Cleveland: Chemical Rubber Co.).

Handbook of Mathematical Functions 1964, ed. M. Abramowitz and I. A. Stegun (Washington, D.C.: National Bureau of Standards).

Herzberg 1945, Infrared and Raman Spectra of Polyatomic Molecules (Princeton, New Jersey: Van Nostrand Co.).

Hess, S. L. 1953, Ap. J., 118, 151.

Ho. W., Kaufman, I. A., and Thaddeus, P. 1966, J. Geophys. Res. 71, 5091.

Hogg, D. C. 1959, J. Appl. Phys., 30, 1417.

Hubbard, W. B. 1968, Ap. J., 152, 745.

International Critical Tables 1928 (New York: McGraw-Hill Book Co.), vol. 3.

Kalaghan, P. M., and Wulfsberg, K. N. 1968, Ap. J., 154, 771.

Kislyakov, A. G., and Lebskii, Yu. V. 1967, Soviet Astr.-AJ, 11, 561.

Kuiper, G. P. 1952, in The Atmospheres of the Earth and Planets, ed. G. P. Kuiper (Chicago: University of Chicago Press), p. 306.

Lasker, B. M. 1963, Ap. J., 138, 709.

Law, S. E. and Staelin, D. 1968, Ap. J., 154, 1077.

Loewenstein, E. V. 1960, J. Opt. Soc. Am., 50, 1163.

Low, F. J. 1965, Lowell Obs. Bull., No. 128, 6, 184.

———. 1966, A. J., 71, 391.

Low, F. J. and Davidson, A. W. 1968, paper presented at the 128th meeting Am. Astr. Soc., Austin, Texas, December 10, 1968.

Mayer, C. H., McCullough, T. P., and Sloanaker, R. M. 1958, Ap. J., 127, 11.

Moroz, V. I. 1966, Soviet Astr.-AJ, 10, 457.

Morris, D., Whiteoak, J. B., and Tonking, F. 1968, Aust. J. Phys. 21, 337.

Mould, H. M., Price, W. C., and Wilkinson, G. R. 1959, Spectrochimica Acta, 15, 313.

Münch, G., and Younkin, R. L. 1964, A. J. 69, 553.

NBS Circular 518, 1952, Molecular Microwave Spectra Tables (Washington, D.C.: National Bureau of Standards).

NBS Circular 564, 1955, Tables of Thermal Properties of Gases (Washington, D.C.: National Bureau of Standards).

Naumov, A. P. and Khizhnyakov, I. P. 1965, Soviet Astr.-AJ, 9, 480.

Nielsen, A. H. and Nielsen, H. H. 1935, Phys. Rev., 48, 864.

Öpik, E. J. 1962, Icarus, 1, 200.

Owen, T. 1965a, Ap. J., 141, 444.

———, 1965b, ibid., 142, 782.

Owen, T., and Mason, P. 1968, Ap. J., 154, 317.

Owen, T., and Walsh, T. E. 1965, Nature, 208, 476.

Owen, T. and Woodman, J. H. 1968, Ap. J. 154, L-21.

Plass, G. N. 1958, J. Opt. Soc. Am., 48, 690.

———. 1960, ibid., 50, 868.

Pollack, J. B. 1968 (private communication).

Rank, D. H., Fink, U., and Wiggens, T. A. 1966, Ap. J., 143, 980.

Rose, W. K., Bologna, J. M., and Sloanaker, R. M. 1963, Phys. Rev. Lett., 10, 123.

Sagan, C. 1968, Science, 159, 448.

Sakurai, K., and Shimoda, K. 1961, J. Phys. Soc. Japan, 21, 1842.

Schwarzschild, M. 1958, Structure and Evolution of the Stars, (Princeton, New Jersey: Princeton University Press).

Spinrad, H. and Trafton, L. M. 1963, Icarus, 2, 19.

Squires, P. 1957, Ap. J. 126, 185.

Stecher, T. P. 1965, Ap. J. 142, 1186.

Tanaka, W. 1966, Pub. Astr. Soc. Japan, 18, 339.

Taylor, D. J. 1965, Icarus, 4, 362.

Teifel, V. G. 1966, Soviet Astr.-AJ, 10, 121.

Thornton, D. D., and Welch, W. J. 1963, Icarus, 2, 228.

Townes, C. H., and Schawlow, A. L. 1955, Microwave Spectroscopy (New York: McGraw-Hill Book Co.).

Trafton, L. M. 1965, unpublished Ph.D. Thesis, Calif. Inst. Tech.

———. 1966a, Ap. J., 146, 558.

———. 1966b, (private communication).

———. 1967, Ap. J., 147, 765.

———. 1968, (private communication).

Walker, R. G. 1966, unpublished Ph.D. Thesis, Harvard University.

Wildey, R. L. 1964, Icarus, 3, 332.

————. 1968, Ap. J., 154, 761.

Winter, S. D. 1964, Expected Microwave Emission from Jupiter at Wavelengths Near 1 cm., University of California Space Science Lab., Technical Note, Series 5, Issue 23.

Wright, N., and Randall, H. M. 1933, Phys. Rev., 44, 391.

VITA

Gary Charles Goodman was born on April 16, 1938, in Mount Vernon, New York. He attended the California Institute of Technology at Pasadena, California from 1956 to 1960 and received the B.S. degree in astronomy in June, 1960. From 1960 to 1969 he attended the University of Illinois at Urbana, Illinois, and received the M.S. degree in astronomy in February 1964. From 1960 to 1968 he held an assistantship in the astronomy department, almost all of it in teaching.